Slow G-Quadruplex Conformation Rearrangement and Accessibility Change Induced By Potassium in Human Telomeric Single-Stranded DNA.

Running title: Slow G-quadruplex refolding in potassium

Arianna N. Lacen, Andrew Symasek, Alan Gunter, and Hui-Ting Lee*

Department of Chemistry, University of Alabama at Birmingham
901 14th street South, Birmingham, Alabama, USA 35294

*Corresponding author: htlee@uab.edu

ABSTRACT

The guanine-rich telomeric repeats can form G-Quadruplexes (G4s) that alter the accessibility of the single-stranded telomeric overhang. In this study, we investigated the effects of Na^+ and K^+ on G4 folding and accessibility through cation introduction and exchange. We combined differential scanning calorimetry (DSC), circular dichroism (CD), and single molecule Förster resonance energy transfer (smFRET) to monitor the stability, conformational dynamics, and complementary strand binding accessibility of G4 formed by single-stranded telomeric DNA. Our data showed that G4 formed through heating and slow cooling in K^+ solution exhibited fewer conformational dynamics than G4 formed in Na^+ solution, which is consistent with the higher thermal stability of G4 in K^+. Monitoring cation exchange with real time smFRET at room temperature shows that Na^+ and K^+ can replace each other in G4. When encountering high K^+ at room or body temperature, G4 undergoes a slow conformational rearrangement process which is mostly complete by two hours. The slow conformational rearrangement ends with a stable G4 that is unable to be unfolded by a complementary strand. This study provides new insights into the accessibility of G4 forming sequences at different time points post introduction to a high K^+ environment in cells, which may affect how the nascent telomeric overhang interacts with proteins and telomerase.

INTRODUCTION

The telomeric DNA is composed of species-specific tandem repeats that are called telomeric repeats. In vertebrates, telomeric DNA is composed of a guanine-rich (G-rich) strand that has thousands of 5'-TTAGGG sequence and a complementary cytosine-rich (C-rich) strand. The G-rich strands extend over the C-rich strand by 100–200 nucleotides (nt), creating a G-rich 3' single-stranded DNA (ssDNA) overhang[1-3]. The repetitive GGG in the telomeric DNA G-rich strand can form the non-canonical secondary structure G-quadruplex (G4). G4s are comprised of G-tetrads, which is formed by four guanine bases arranged planarly through Hoogsteen hydrogen bonding and stabilized by a monovalent cation at the center[4, 5], as shown in **Scheme 1**. The vertebrate telomeric G-rich DNA forms G4 with three stacks of G-tetrads at the center and the sugar-phosphate backbone pointing outward, which leaves the non-guanine TTA sequence between the GGG sequences as "loops" surrounding the stacking G-tetrads. G4 has been considered a promising drug target due to its special structure, high thermal stability, and its presence in telomeres as well as many promoter regions (see recent reviews by Varshney et al.[6] and Kosiol et al.[7]).

G4s can form in different conformations based on the 5' to 3' orientations of the phosphate backbones of each GGG strand[8]. G4s can have each strand in the same direction (parallel G4), alternating direction every other strand (antiparallel G4), or in any of the direction (broadly known as

mixed or hybrid conformations)[5, 9-11]. Differences in G4 stability and accessibility of G4-forming sequence has been associated with different G4 conformations[5, 12-15], which affects the interaction between telomeric DNA and proteins that regulate telomere structure and maintain telomere length[13, 16-27]. G4 stabilities have been well investigated in attempt to explain the interaction between G4 forming sequences and the proteins or drugs interacting with them. It has been found that well-folded G4s are resistant to unfolding and require higher force to unfold than duplex DNA[28, 29]. Since G4s have been found to be highly stable, it is important to understand their formation and subsequent interactions with other cellular components.

Considering the physiological environment surrounding the telomere G4, and the proposed interaction between telomeric overhang and proteins, the stability of G4 may play a critical role in terms of ssDNA accessibility. From a thermodynamic point of view, the binding of telomerase or the ssDNA binding protein POT1 to telomere ssDNA needs to provide a more favorable free energy than the formation of telomeric G4. From a kinetic point of view, POT1 and telomerase need to form noncovalent interactions with the bases in telomeric DNA through the atoms that are used for G4 formation. All the existing telomeric G4 structures, parallel (PDBID: 6IP3), antiparallel (PDBID: 5YEY), and hybrid (PDBID: 2JPZ), [10, 30, 31] show that the guanines are stacked on top of each other and surrounded by stacking loop sequences, which make it difficult to access the guanines. Therefore, the binding may require a tentative unfolded state of G4 to allow the binding domain in the proteins to reach the desired atoms in DNA bases.

However, there are mixed reports regarding the G4 conformation and accessibility. For example, many reports based on NMR, circular dichroism (CD), and other methods show telomeric G4 to be highly polymorphic in potassium ion (K^+) [29, 32-35], but there are other reports that demonstrate limited G4 conformations in K^+ [14, 36]. Another example is that the ssDNA binding shelterin protein POT1 was reported to bind to the telomere G-rich DNA that formed G4[20, 27] but stable telomeric DNA G4 was also reported to block POT1 binding[14]. The contradictory reports on conformation polymorphism and accessibility make it difficult to predict the true behavior of G4 in cells. One possible set of parameters contributing to the contradictory results is the G4 folding kinetics. The reported folding rate of intramolecular G4 spans from milliseconds to minutes[37-39], whereas formation of intermolecular G4 takes hours to days in sub-millimolar strand concentration[40, 41]. Biophysical studies showed that telomeric ssDNA forms G4 and undergoes conformational rearrangement for hours after an initial rapid folding[39, 42]. The broad range of folding rate and complex folding path implies that folding or conformational rearrangement may persist for hours. This G4 conformational rearrangement may work as a mechanism for kinetic control of the cell cycle. Characterizing G4 conformational rearrangement would provide new insight into cell cycle regulation. Moreover, if conformational rearrangement regulates DNA accessibility, new drugs can be designed to target the genomic regions that undergo conformational rearrangement.

In this study, we investigate the G4 structural and conformational dynamics in the presence of Na^+, K^+, and a mixture of the two. The ensemble thermal stability and conformation of G4 were investigated by DSC and CD, respectively. The conformational dynamics and complementary strand accessibility of G4 were monitored in real-time by single molecule Förster resonance energy transfer (smFRET). Our data suggests that the high stability and low accessibility of G4 in K^+ are associated with low conformational dynamics. A G4 forming sequence goes through a rapid folding while encountering K^+ and a slow conformational rearrangement which lasts for two hours or longer to complete. Once the conformational rearrangement stops and a stable G4 is formed in the presence of high K^+, the stable G4 cannot be unfolded by a complementary strand of half length. These results provide a new insight into the role of different G4 conformations in the ensemble accessibility of telomeric DNA.

METHODS

DNA oligonucleotides

All oligonucleotides were purchased from Integrated DNA Technologies (IDT, Coralville, IA) with HPLC purification. The dyes were covalently attached to either 3'-OH groups of oligonucleotides through a six-carbon (C6) linker or inserted into the DNA backbone between the phosphate group and the ribose C5 of indicated bases (see Table 1). The DNA G4 with a partial double-stranded (ds) handle was generated by annealing each DNA with a biotin-conjugated 18-mer DNA strand in a molar ratio of 1:1. Each 10 μL sample was mixed in 10 mM Tris-HCl (pH 7.5) and either 100mM NaCl or 100 mM KCl then heated at 95 °C for 5 min, cooled to 48 °C at a rate of 1°C per minute, and then to room temperature at a rate of 4 °C/min as reported earlier[14].

Differential Scanning Calorimetry (DSC)

DSC thermograms were collected using a MicroCal VP-DSC. 80 to 100 μM of sample was annealed in 10mM Tris-HCl pH 7.5 and either 100mM NaCl or 100mM KCl then heated from 4 °C to 95 °C at a scan rate of 60°C/hr and then cooled to measure the reversibility of the folding transition. Resulting thermograms were subtracted from the heats of the buffers and then fit using a two-state model to find the T_m and ΔH of the melting transition. ΔG at 25 and 37 °C was calculated from ΔH and T_m using Eq. (1)[43]:

$$\Delta G = \Delta H \times (1 - \frac{T}{T_m}) \qquad (1)$$

Circular Dichroism (CD)

CD spectra were collected using a Jasco J-815 spectrophotometer equipped with a Jasco PTC-517 Peltier temperature controller using a quartz cuvette (1 cm path length) at 25°C. The DNA concentration was between 80 to 100μM. Samples were annealed in 10mM Tris-HCl pH 7.5 and either 100mM KCl or 100mM NaCl as described above. Scans were conducted between 200–320 nm with 3 accumulations

acquired at a scan speed of 50 nm/min, then blank-corrected with the data from the corresponding buffer without DNA. The spectra were normalized to molar concentration of each sample DNA. Cation exchange experiments in CD were done by adding sufficient volume of concentrated replacement buffer to the sample cuvette in the original buffer. Spectra were collected at timepoints specified in the FRET salt replacement assays. Temperature dependent CD was performed with 24 μM No-Handle-4R-TTAG annealed in 100 mM KCl, 10 mM Tris-HCl, pH 7.5 and heated from 5°C to 95°C with a rate of 1°C/min, with scans from 220 to 320 nm taken every five degrees. Once heated to 95°C, it was reversibly cooled back to 5°C at the same rate, with scans from 220 to 320 nm taken every five degrees.

Single-molecule FRET (smFRET)

All single-molecule assays were performed with a home-built prism-type total internal reflection fluorescence (TIRF) microscope with solid-state 532 nm and 637 nm OBIS lasers (Coherent, Saxonburg, PA) at room temperature. The coverslips and quartz slides were passivated with a mixture of m-PEG-5000 and biotin-PEG-5000 (Laysan Bio, Inc, Arab, AL) in a weight ratio of 40:1 as reported earlier[44]. DNA samples were immobilized on to PEGylated surface via biotin-neutravidin interaction in 10 mM Tris pH 7.5 and either 100 mM KCl or 100mM NaCl. The data was collected in an imaging buffer (10 mM Tris, 100 mM KCl or NaCl, 1 mg/mL glucose oxidase, 0.5% v/v glucose, 10 mM Trolox, and 2 μg/mL catalase) that generated an oxygen scavenging system. The imaging buffer was prepared by mixing 10 mM Trolox solution with desired Tris and KCl/NaCl salt, then adding glucose and glucose oxidase. It is noteworthy that 10 mM Trolox solution was prepared with NaOH or LiOH to enhance the solubility of Trolox. Trolox prepared with NaOH was used in most of the smFRET experiments except for Tris-only experiments, in which we used Trolox prepared in LiOH instead. Data were acquired with an EMCCD camera at 100 ms per frame rate and further processed using IDL and MATLAB codes. FRET efficiency (*E*) and stoichiometry (S) were calculated according to *Eq* (2) and (3)

$$E = \frac{F_A^D}{F_D^D + F_A^D} \qquad (2)$$

$$S = \frac{F_A^D + F_D^D}{F_A^D + F_D^D + F_A^A} \qquad (3)$$

where F_A^D is the acceptor (*A*) signal upon the donor (D) excitation; F_D^D is the direct excitation of *D*; and F_A^A is the direct excitation of A [44, 45]. Each FRET histogram was generated from 20 individual movies that collectively contained 5000-6000 molecules with a Cy3-Cy5 pair. FRET histograms were further fitted into Gaussian distribution functions using Origin 2022 software.

smFRET Salt Replacement Assays

DNA samples were immobilized on to the PEGylated surface after being annealed in 10mM Tris-HCl (pH 7.5) and either 100mM KCl or 100mM NaCl. Initial data was collected in imaging buffer as described above. 200 μL of imaging buffer containing 10mM Tris-HCl and various concentration ratios of

NaCl and KCl was injected into the slide using tubing connected to a vacuum pump for complete injection by 5 seconds. Samples were monitored over 2 hours with timepoints being taken every 5 minutes for 30 minutes then at each hour. Histograms were generated as described above.

smFRET C2 Binding Assays

DNA samples were immobilized on to the PEGylated surface after being annealed in 10mM Tris-HCl (pH 7.5) and either 100mM KCl or 100mM NaCl. Initial data was collected in imaging buffer as described above. At various times of cation incubation, 200 µL of imaging buffer containing 10mM Tris-HCl, 100 mM of NaCl and KCl, and 1 µM C2 ($(CCCTAA)_2$) was injected into the slide using tubing connected to a vacuum pump for complete injection by 5 seconds. Timepoints were taken at immediate co-introduction of cation and C2, 5 minutes of cation incubation then introduction of C2, and so on for 10, 15, 20, 30, 60 and 120 minutes. Real time flow in movies were collected at the addition of C2. Histograms were generated as described above.

RESULTS AND DISCUSSION

Construct Design and smFRET Signal Interpretation.

The G4 forming DNA constructs used in smFRET experiments contain Cyanine3 (Cy3) and Cyanine5 (Cy5) dyes, which serve as a FRET donor and acceptor pair respectively. All constructs are composed of the same biotinylated non-telomeric double stranded DNA (dsDNA) handle region and a ssDNA region that forms G4. The G4 forming strand contains the complementary handle sequence followed by four to five repeats of the telomeric G-rich sequence and a Cy3. The construct 4R contains four repeats of TTAGGG, immediately followed by the Cy3 at the terminal 3'-OH. The position of the Cy3 dye was chosen to not perturb G4 formation by interrupting the four consecutive TTAGGG repeats. 4R-TTAG contains four repeats of TTAGGG, followed by the Cy3, and ends with a truncated telomeric repeat sequence, TTAG. 4R-1R contains four repeats of TTAGGG, followed by the Cy3, and then another full repeat of TTAGGG. The dsDNA handle has the Cy5 located between the 4^{th} and 5^{th} bases from the dsDNA-ssDNA junction (see Scheme 1). This Cy5 dye position allows for sensitive detection of G4 conformational change [46], as opposed to other labeling positions that only detect folding and unfolding of G4[47] . The orientation of the fourth TTAGGG repeat determines the distance between the Cy3 and Cy5 dyes. In G4s containing five repeats of telomeric G-rich sequence, this Cy5 position can be also used to detect the FRET differences between 3' and 5' folded G4s[14, 46]. We used the truncated version of the three G4 constructs that retained the telomeric sequence but did not have the handle sequence or the Cy3 to eliminate any contribution that they may have on either the T_m in DSC or on structure in CD.

We characterized the G4 compactness and conformational dynamics in each salt solution using smFRET. Each DNA construct was annealed in buffers containing 100 mM KCl or 100 mM NaCl by heating to 95 °C and slow cooled as described in Material and Methods. In general, each construct has higher FRET efficiency in KCl than in NaCl. As shown in the smFRET histograms in Figure S1, 4R and 4R-TTAG each exhibited a single population in KCl and NaCl, centered at FRET efficiency (E) of 0.71 ± 0.03 in KCl and of 0.62 ± 0.03 in NaCl. The smFRET histograms of 4R-1R exhibit multiple population in KCl with two peaks centered at E of 0.62 ± 0.02 and 0.45 ± 0.02, similar to earlier reports by our group which identified the two populations to be using the first or last four GGG in the 4R-1R construct, which were assigned as 5' or 3' G4[46]. Interestingly, 4R-1R only displayed one major population in NaCl, centered at 0.60 ± 0.02 E but spread across the same FRET efficiency range of the two peaks in KCl and with a minor population centered at 0.80 ± 0.02 E. This broad distribution of FRET efficiency value may indicate a mixture of 5' G4 and 3' G4 at different ratios (e.g., lower 5', 3', or long-loop G4) in NaCl or overlapping hybrid and antiparallel G4 population. Thus, the presence of the fifth repeat may prevent 4R-1R from folding into the same conformation as 4R and 4R-TTAG, as folding at the 3' end with the larger loop may limit the conformations it can adapt.

K^+ G4 Has Higher Thermal Stability and Less Conformational Dynamics.

To characterize the effect of cations on thermal stability of G4, we conducted DSC experiments on DNA constructs similar to the ones used in smFRET but without the Cy3, Cy5, and the dsDNA handle sequence (handle-free constructs), named No-Handle-4R, No-Handle-4R-TTAG, and No-Handle-5R (Table 1). DSC scans were conducted on 80-100 μM of each handle-free construct in buffer containing 100 mM of either KCl or NaCl and 10 mM Tris-HCl at pH 7.4. Six or more scans were conducted with each construct from 4°C to 95 °C at a rate of 60°C/hr. After each heating scan, the sample was allowed to cool back down to 4°C at the same rate. The first scan mimics the annealing step before smFRET experiments. For this reason, we only compare the second and later DSC scans with the data collected with smFRET. Representative DSC thermograms for No-Handle-4R-TTAG and No-Handle-5R are shown in Figure S2B. In freshly prepared samples, all the scans of the each sample have one distinct peak at the same melting point (T_m) and with the same enthalpy (ΔH), indicating no heat-induced DNA damages and persisting folded structure formation. DSC scans were also conducted with scan rates of 30, 45, and 90 °C/hr. The change in scan rates does not change the T_m. The only differences noted between scan rates was the broadness of the peak, notable only at the 90°C/hr scan rate where the peak was broader (Figure S3A). Cooling scans were collected but not analyzed due to the inability to capture a recognizable folding transition, instead showing a broad curve (Figure S3A). Changing the cooling scanning rate also did not allow a peak to be seen, indicating that the folding process is too slow to be detected by the 60°C/hr cooling rates in our DSC experiment, or happened through the full temperature range of scan

and the overlapping “folding transitions” made the DSC cooling curves too broad to be analyzed. The inability to capture the folding transition in DSC was unexpected and suggests that G4 folding is a slow process and may not proceed through a standard 2-step process as unfolding. It may instead proceed through a series of intermediates, as suggested earlier[39].

In agreement with previous reports on G4s[48, 49], our DSC data for each construct annealed in buffer containing 100 mM KCl exhibit higher melting temperatures and enthalpies than their NaCl annealed counterparts (Figure S1C). No-Handle-4R, No-Handle-4R-TTAG, and No-Handle-5R have a single transition with a T_m of 61 ± 1 °C, 58 ± 2 °C, 56 ± 2 °C in KCl as opposed to 50 ± 2 °C, 43 ± 1 °C, and 45 ± 1 °C in NaCl, respectively (see Table 2). The T_m of No-Handle-4R-TTAG in KCl and No-Handle-4R-TTAG in NaCl are consistent with reports from other groups on the same or similar sequence [50 51]. The trend in melting temperature follows that the fewer number of repeats available to form a G4, the greater the thermal stability (Figure S2B). This trend is consistent with the reports from the field that the extra bases beyond the four GGG tracts change the conformation of G4 [52, 53]. This can be explained by the model that more repeats available to form G4 increases the risk of folding into an unstable conformation. Similar to T_m, the unfolding enthalpy of each construct is also higher in KCl than in NaCl. In KCl, No-Handle-4R, No-Handle-4R-TTAG, and No-Handle-5R have a ΔH_{cal} of 47 ± 2, 53 ± 3, and 52 ± 2 kcal/mol, respectively. While in NaCl, the ΔH_{cal} lowers to 40 ± 3, 39 ± 2, and 43 ± 2 kcal/mol. Each melting transition occurred in a two-state manner, with no obvious intermediate melting states. For example, KCl annealed No-Handle-5R has a ΔH_{cal} of 52 kcal/mol and a ΔH_{VH} of 46 kcal/mol, giving a $\Delta H_{VH}/\Delta H_{cal}$ ratio of 0.9, supporting a two-state transition. This is in stark contrast to the cooling scans where the transition spread across the whole temperature scanning range that no obvious transitions could be seen. Such a broad transition would indicate that the G4 formation, or folding, proceeds through many intermediates across the scanned temperature range, with the folding peak of the intermediate states overlapping with each other.

To confirm that the presence of a Cy3 dye does not affect the thermal stability of the G4, DSC melting experiments were also conducted on (1) fluorescently labeled handle-free constructs with Cy3 and (2) constructs with polyethylene glycol spacers replacing Cy3 in the DNA backbone. The melting points did not differ depending on the presence of either spacer or dye. Details of this experiment can be found in Table S1 and the Supplementary Results.

Prolonged Storage at High Concentration and Low Temperature Favors Intermolecular G4.

To further investigate the effect of time on G4 folding, we kept the DNA sample in the DSC cells at 4 °C after the initial heating and cooling scans, then performed the same heating and cooling scans after 48 hours of storage at 4 °C. We noted that DNA samples held at 4 °C for two days showed another peak with a lower T_m. Freshly prepared 210 μM No-Handle-4R-TTAG in NaCl had a single peak at 43 ±

1 °C but after 48 hours of 4 °C storage, the first scan had an additional peak at approximately 23 ± 2 °C, followed by the peak with the same T_m as the freshly prepared sample (see Figure S3C). When the DSC scan after 48 hours storage was done with 41 μM of the same construct, the peak with lower T_m disappeared but the peak with a higher T_m of 43 °C remained unchanged. This data shows that the long storage at low temperature allows the formation of intermolecular G4 structure that has a lower T_m. This data is consistent with reports on high strand concentrations ($C_t \geq 35$ nM) favor intermolecular G4 formation[54]. Because the 43 °C peak remained unchanged regardless of C_t, we can safely assign it to be the desired intramolecular G4 we studied using smFRET, as smFRET samples were annealed at 10 μM of G4 forming strand.

Each G4 Forming Construct Exhibits Expected Conformation in Either NaCl or KCl.

CD spectra were collected to investigate the conformation of each construct. 80 to 100 μM of each handle-free constructs was annealed in buffer containing either 100 mM NaCl or KCl with 10 mM Tris-HCl as described in the methods. The spectra were collected from 200–320 nm at room temperature, 25 °C. Multiple X-ray, MNR, and CD reports on G4 have assigned the most common or preferred conformation of the human telomeric G4 to be antiparallel in NaCl and a mix of hybrid-1 and hybrid-2 in KCl[5, 50, 55]. All G4 constructs in 100 mM NaCl exhibited a CD spectrum identical to reported antiparallel G4 conformation, with positive peaks at 295 and 240 nm and a negative peak at 260 nm. While the negative 260 nm peak is prominent in No-handle-4R and No-handle-4R-1R, it is considerably shallower in No-handle-4R-TTAG. Although the shallow 260 nm CD peak may lead to the assumption that No-handle-4R-TTAG is less folded, comparative work by others using CD on G4 structure have repeatedly demonstrated fluctuations in the intensity of the characteristic peaks, depending on the loop sequence and the extra bases beyond the G4 core [52, 53, 56]. The antiparallel G4 conformation of a sequence similar to our No-handle-4R-TTAG in NaCl was confirmed using CD, 1D and 2D NMR[33]. All the constructs in 100 mM KCl exhibited a CD spectrum identical to reported hybrid conformation, with positive peaks at 295 and 260 nm and a negative peak at 240 nm (Figure S1D and S2C). Cy3-labeled and spacer constructs gave the same CD spectra. To confirm that the G4s were melting and refolding reversibly, we performed temperature dependent CD spectroscopy. (Figure S3B). Plotting the CD signal at 295 nm versus temperature shows a melting and folding temperature that exactly matches what was seen in the DSC, confirming our earlier results (Figure S3D). We also see the reversibility of the reaction using the cooling curve at 295 nm, which gives a folding temperature of 58 °C and is similar to the melting temperature. In CD, because the signal comes from plane polarized light, it sensitively captures the transition between randomly distributed versus orientated guanines at 295 nm. In contrast, in DSC, the heat capacity change of intermediates along the cooling/folding path are broad and overlapping, leading to the absence of any noticeable peak. This difference in CD and DSC cooling curves further supports

our hypothesis of slow refolding. Thus, DSC and CD confirm that the constructs used in smFRET exhibited expected conformations and stability after the initial annealing process.

Based on the CD spectra in either NaCl or KCl, we assign for 4R and 4R-TTAG that the 0.62 ± 0.02 E population in the NaCl smFRET histogram is the antiparallel conformation and the 0.71 ± 0.02 FRET in KCl is a hybrid conformation. The higher FRET efficiency in KCl, which is translated to a shorter end-to-end distance, can be attributed to a more compact K^+ G4. On the other hand, although CD spectra of 4R-1R also showed the signature of antiparallel G4 in NaCl and hybrid G4 in KCl, it is challenging to assign conformations to the two populations in the smFRET histogram. It is possible that the bimodal histogram results from hybrid-1 and hybrid-2 structures using different GGG repeats. The difficulty complicates further studies into dynamic behavior and refolding, thus we focus on the constructs that have four full TTAGGG repeats. 4R and 4R-TTAG that in KCl have identical high FRET peaks in smFRET histograms and exhibit similar thermodynamic profiles in each salt (Figure S1A). We thus focus on 4R-TTAG to characterize the folding and refolding behavior of a single G4 in the salt induced refolding experiments in the next section.

The difference in FRET between the KCl annealed and NaCl annealed constructs agrees with previous work indicating that K^+ allows the G4 to form a more compact conformation that is resistant to unfolding[50, 57]. Besides the higher T_m and ΔH observed through thermal unfolding, AFM studies also showed that more force is required to unfold K^+ G4s than Na^+ G4s formed with the same sequence[29, 58]. To better elucidate the cause of this stability difference shown in ensemble methods, we analyzed the conformational dynamics of individual G4s using real-time smFRET. We compared conformational dynamics of constructs annealed in a buffer containing 100 mM NaCl (NaCl annealed G4s) with the constructs annealed in a buffer containing 100 mM KCl (KCl annealed G4s) at 25°C. To quantify the conformational dynamics, we performed trajectory type count on the long smFRET movies as reported earlier[14, 46, 59]. A dynamic trajectory is defined as a trajectory that underwent at least one FRET efficiency change beyond the ~0.03 E instrumental noise (FRET transition) within the 2 minutes recording time. The trajectories that did not show any FRET transitions during the 2 minutes recording time are defined as static trajectories. In NaCl, dynamic trajectories account for approximately 15% of all molecules for 4R-TTAG and approximately 25% for 4R-1R. In comparison, KCl annealed 4R-TTAG has approximately 6% dynamic trajectories, while 4R-1R has approximately 5% (Figure 1A). The higher amount of dynamic trajectories in NaCl than KCl indicates that NaCl annealed G4s more frequently have changes in the end-to-end distance, possible through structural rearrangements of the G4 that are not present in KCl at room temperature.

G4 Undergoes Constant Refolding Near the Melting Point.

It is important to note that the intramolecular G4 melting temperatures obtained for each cation type is significantly higher than the room temperature (~25 °C) that smFRET was initially conducted in. 25°C is also at the beginning of the melting transition for the NaCl annealed DNA constructs (see Figure S1C, S2B). To evaluate how the temperature difference between smFRET operating temperature and T_m affects conformational dynamics, smFRET studies were conducted at 37°C for each construct in 100 mM NaCl or KCl. As shown in Figure S4, the smFRET histogram of 4R-TTAG exhibited bimodal behavior in NaCl with two peaks at 0.45 ± 0.02 and 0.61 ± 0.02 FRET and monomodal behavior in KCl with a peak at 0.66 ± 0.02 FRET. 4R-1R exhibited similar behavior to 25 °C in NaCl with one major peak centered at 0.64 ± 0.03 FRET and a broad low FRET shoulder centered at 0.50 ± 0.02 FRET. In KCl, 4R-1R still exhibits bimodal distribution with two peaks centered at 0.63 ± 0.02 and 0.52 ±0.03 FRET (Figure S4A). The most striking difference exists between 4R-TTAG in NaCl at 25 °C and 37 °C, which can be explained by the proximity to its T_m of 43 ± 1°C, which would mean that at 37 °C, close to 50% of the G4s would be melted. Classical definitions of melting assumes that a “melted” or thermally denatured G4 exists as linear ssDNA and an “unmelted” or thermally intact G4 exists as a folded structure. It is hard to use ensemble methods to measure whether a tube of DNA at its melting point has all of the molecules in 50% partial-unfolded state, or 50% of the molecule in unfolded state and 50% in folded state. For example, the two peaks present in a bimodal distribution such as in Figure S4A left panel could correspond to (a) each molecule spent equal time fluctuating between folded (0.62 E) or unfolded state (0.45 E) during recording, (b) ~50% of the molecules stayed folded statically and ~50% stayed unfolded statically during recording, or (c) a mixture of these two scenarios. Analysis of smFRET trajectories in NaCl at 37°C provides a clarification of G4 structural behavior, revealing that the two peaks seen in the smFRET histogram are actually the result of near constant fluctuations between 0.45 and 0.62 FRET efficiency, not two distinct populations of folded or unfolded (Figure S4E). Figure S4C shows that at 37°C, NaCl annealed 4R-TTAG has the majority of trajectories being dynamic while KCl annealed 4R-TTAG has a majority of trajectories in a static high FRET efficiency state, similar to 25°C. The peak center of the KCl histograms is lower, at 0.66 ± 0.02 E at 37°C versus 0.71 ± 0.03 E at 25°C, indicating that the increased temperature may slightly increase the end-to-end distance of 4R-TTAG, although most trajectories are still in a high FRET state statically (Figure S4A). Therefore, we propose the definition of G4 T_m in NaCl to be the temperature at which the majority of the molecules adopt a looser conformation that is capable of refolding and spends half of the time in the folded state.

G4 At Equilibrium Has a Broader Conformational Distribution and Spends More Time in Unfolded States In Na^+.

It is hard to explain the -14 ± 4 kcal/mole more favorable ΔH and the 15 ± 4 °C increase of T_m (overall more favorable ΔG of -14 ± 4 kcal/mole) at 25 °C of 4R-TTAG from NaCl to KCl with only 9% fewer dynamic trajectories. Therefore, we investigated the refolding path and the time each molecule stays at each state. Analyzing the beginning and ending FRET efficiency levels for each smFRET transition can reveal a path preference for either a folding or unfolding event, which may differ between constructs. To examine this behavior, transition density plots (TDP) were created by plotting the beginning FRET efficiency of each dynamic event against the ending FRET efficiency of the event. The TDPs of each construct annealed in buffer containing 100 mM KCl or NaCl show symmetric distribution of the transient event on the two sides of the diagonal line, which indicate that there is no preference for a pathway during folding/unfolding events (Figure 1B). Thus, path preference cannot explain the observed differences in T_m and ΔH.

The TDP in Figure 1B shows that K^+ annealed 4R-TTAG has transitions clustering within a narrow range of 0.65 ± 0.05 E to 0.80 ± 0.05 E, whereas Na^+ annealed 4R-TTAG has a broader range from 0.50 ± 0.05 E to 0.80 ± 0.05 E. 4R-1R however, has a broad FRET range from 0.60 ± 0.05 to 0.80 ± 0.05 in KCl and from 0.40 ± 0.05 to 0.70 ± 0.05 in NaCl. This data indicates that the more telomeric repeats available to form a G4, the more conformations it samples, leading to the observed broader FRET efficiency distribution seen for 4R-1R than 4R-TTAG. 4R-1R has a broader distribution in both NaCl and KCl, indicating that not the cation type but rather the number of telomeric repeats is responsible for the conformational heterogeneity difference between 4R-1R and 4R-TTAG. This finding agrees with the DSC data in which fewer repeats available for folding leads to greater thermal stability. Overall, the TDPs reveal that, compared to the KCl annealed G4, NaCl annealed G4 unfolds to conformations with a longer end-to-end distance and has a broader range of conformations it unfolds and refolds to. Therefore, the difference in stability stems from the higher degree of conformational heterogeneity.

While the number of dynamic trajectories differs between cations, the length of time each molecule spent on each state of same continuous FRET efficiency (FRET state) is also different. In K^+, the FRET transitions are fewer in each dynamic trajectory and each FRET state lasts for longer periods of time than in Na^+ (Figure 1A). Quantification of the time spent at each FRET state are shown in dwell time plots, which show the duration of the first ten FRET states. The dwell time plots in Figure 1B show that each construct in each salt exhibits a rapidly fluctuating population lasting under 20 seconds. This rapidly fluctuating population is greater in Na^+ than it is in K^+, from 80-100 events in Na^+ to 30-40 in K^+, supporting the notion that K^+ is a better stabilizing cation. K^+ does not *stop* dynamic behavior from occurring, it simply *reduces* the frequency as K^+ holds two G-tetrads together and raises the energy barrier of G4 to unfold and refold. Constructs annealed in K^+ also exhibit more transitions lasting longer than 20 seconds than the Na^+ annealed constructs. The long lived “transitions” at 120 seconds are static

trajectories that do not undergo FRET transitions but were included in the analysis to show that the frequency of stable trajectories is higher in KCl than in NaCl.

K^+ Induces Conformational Change to a More Compact State.

Having established that the NaCl annealed G4s have higher dynamics and lower thermal stability than the KCl ones, we turned next to the dynamic behavior caused by Na^+ to K^+ cation exchange (K^+ exchange). Sodium is less capable of stabilizing G4 than potassium, with rationales stemming from the smaller size of Na^+, the less favorable Na^+ G4 folding free energy, and the higher hydration energy of Na^+ as determined by NMR[60]. Earlier mass spectrometry studies on Na^+ to K^+ cation exchange in G4 suggested that K^+ can replace Na^+ after dialysis[61, 62]. Thus, we hypothesized that K^+ allows the G4 to adopt a more compact and stable conformation when replacing Na^+ in a folded G4. To study this transition between different G4 conformations, we conducted smFRET cation exchange experiments on both 4R-TTAG and 4R-1R at 25°C. In these experiments, the original imaging buffer containing 100 mM NaCl was replaced by the buffer containing 10 mM NaCl and 100 mM KCl, which is close to the physiological concentrations of NaCl and KCl in the cell. smFRET signal was collected before, during, and after the buffer exchange (see Supplementary Methods.)

As shown by smFRET histograms in Figure 2A, upon replacing NaCl buffer with KCl buffer, both 4R-TTAG and 4R-1R refolded to states with a higher FRET efficiency. For 4R-TTAG, the main peak in NaCl (centered at 0.62 ± 0.02 E) shifted to 0.71 ± 0.03 E with a shoulder centered at 0.80 ± 0.02 E. The main peak stayed centered at 0.71 ± 0.02 E with minimal changes past 5 minutes (Figure S11). The high FRET efficiency shoulder declined and was undetectable by 20 minutes. The increase in FRET efficiency of the main peak to 0.71 E is consistent with the smFRET histograms of KCl annealed 4R-TTAG, which indicates a more compact G4. The short-lived and low proportional nature of the 0.80 E shoulder suggests this population may represent an intermediate state. The sudden introduction of KCl may induce a small population of G4s to “snap” to an intermediate state with a very short end-to-end distance, which later refold into another conformation that has a slightly longer end-to-end distance as the KCl annealed G4. The appearance of the 0.80 E population also helped us to assign a conformation to the 0.71 E main peak. First, since both 4R and 4R-TTAG have this 0.80 E population right after K^+ introduction (see Figure S5), we ruled out the possibility of this 0.80 E population to be an alternative contribution from the TTAG tail. Second, because this 0.80 E population also exists when we directly introduce KCl to a random coil G4 (see data in later sections), we ruled out the possibility of this population to be G4 with both Na^+ and K^+. Third, with the same number of G-tetrads and cation, the only way that a G4 may have shorter end-to-end distance than another G4 is to have a different 5’ to 3’ orientation of the fourth GGG. Therefore, we can assign the 0.71 E main peak to be a G4 with the 3‘ end pointing away from the 5’ end (parallel 4th repeat), and the 0.80 E shoulder has the 3’ end pointing toward the 5’ end (antiparallel 4th repeat). Cation

exchange of 4R-1R exhibited a more complex refolding behavior, which suggests either the refolding process takes longer than the other two constructs, or cation exchange prefers a different conformation than heat-annealing (see Supplementary Result).

Overall, the KCl buffer exchange data support that G4 is capable of forming multiple conformations in KCl. Based on the increase of the 0.71 E population with time (see figure 2A), the conformations with this end-to-end distance may be thermodynamically most favored while other conformations are less favored and slowly refold into the favored conformation. The conformational changes in response to K^+ introduction and incubation were also monitored by a CD titration, where KCl was added into NaCl annealed 4R-TTAG to make 100 mM NaCl and 100 mM KCl, which confirmed that the Na^+ antiparallel G4 refolded into a K^+ hybrid by 60 min (Figure S6).

Cation Exchange at 37°C is Less Efficient than at 25°C

Having previously noted bimodal distributions in NaCl annealed 4R-TTAG at 37°C, we turned to study how increasing the temperature would affect cation induced refolding. We have ascribed the bimodal distribution seen in NaCl annealed 4R-TTAG at 37°C to be the result of frequent unfolding and refolding of the G4 (Figure S4A). Thus at this temperature, the refolding caused by KCl buffer exchange should be easier, as most G4s are unfolded half of the time. Interestingly, the results were significantly different to the 25 °C experiments. At 5 minutes post KCl buffer exchange at 37 °C, the high FRET peak at 0.62 E shifts to 0.66 ± 0.02 E while the lower peak centered at 0.45 E did not shift but had a reduced population ratio (Figure S4B). By two hours post cation exchange at 37°C, there are approximately 40% remaining dynamic behaviors (Figure S4D) as opposed to the almost completely static behaviors seen at 25 °C (Figure 2C). Thus, even though the KCl *annealed* 4R-TTAG histograms and high FRET efficiency trajectory ratios are similar at both 25 and 37°C, the *refolded* KCl 4R-TTAG G4s at each temperature are very different. KCl is not completely capable of "holding together" a G4 at 37°C with the dynamic refolding of Na^+ G4.

Based on the histograms, KCl was capable of lowering the proportion of the 0.45 E state at 37 °C but not to the same magnitude as at 25°C. The higher amount of dynamic behaviors at two hours at 37°C may hint that physiological cation exchange does not lead to G4s that are completely K^+ bound, but instead might be hybrid K^+/Na^+ G4s, thus accounting for the observed increase in dynamic behavior. The 2-hour experimental endpoint was a limitation of our current method (see Supplementary Results), and further study should be conducted to determine if cation induced refolding can reach the same state seen at 25°C. If so, then that would strongly suggest that cation induced refolding is dependent on the starting conformation and can be hindered by kinetic traps that exist along the folding path.

Na^+ to K^+ Cation Exchange Induces Rapid Folding/Refolding Responses.

To better follow the path of conformational rearrangement, we analyzed the smFRET trajectories at different time points of cation exchange at 25°C. Trajectory type count shows that the number of G4s with dynamic behaviors spiked during KCl introduction, then dropped off over time (Figure 2C). Closer analysis of the first 50 seconds after K^+ introduction reveal three distinct behaviors: Behavior 1, FRET efficiency had a sharp drop from 0.62 ± 0.05 E to ~0.45 ± 0.05 E then immediately rose to 0.70-0.80 E; Behavior 2, FRET efficiency increased from 0.60 ± 0.05 E to 0.70-0.80 ± 0.05 E without first dropping to 0.45 E, and Behavior 3, no immediate response to K^+ is noted (Figure 2D).Each behavior counts for 36 ± 2%, 23 ± 5%, and 40 ± 1% of total trajectories respectively. Overall, approximately 60% of G4s responded to K^+ introduction within the first 50 seconds. The 50 second timeframe was chosen because it reflects the time Gray et al proposed for intermediates to form along the folding pathway[39]. The dip to 0.45 E in Behavior 1 is significant because, with this dye-pair position, this value is usually observed for the random coil state of 4R or 4R-TTAG in the absence of Na^+ or K^+ (see Figure 3A)[14]. Therefore, the presence of Behavior 1 indicates some amount of G4 was unfolded to a state similar to random coil and then refolded into G4. In Behavior 1, the duration of the 0.60-0.45 E unfolding event is close to the 0.1 second detection limit of our TIRF microscope, which is consistent with the 0.1 s rate of the initial G4 folding reported by Gray et al[39], while the full 0.60-0.45-0.75 E transition took 0.2 s or slightly longer. Behavior 2 presents a folding path that does not go through an unfolded state during refolding (see Supplementary Result for detail).

The path of the initial conformational rearrangement is quantified in the TDP of the first 3 transitions post KCl buffer introduction (Figure 2D). The asymmetric TDP indicates a preference of folding path. The transitions from ~0.62 E to either 0.45 or 0.75 E (Figure 2D, circle 1-1 and 2) represent the first transition of Behavior 1 and 2, respectively. The 0.45 E to 0.80 E transitions represent the second transition of Behavior 1 (circle 1-2). The 0.45 to 0.80 E transition cluster has a similar density as the 0.62 to 0.45 transition cluster, indicating most of the unfolded molecules folded into a more compact G4 (Behavior 1), which is supported by the low intensity of 0.45 to 0.62 E region. The density of the 0.62 to 0.75 E cluster (circle 2) is only 40% of the clusters of Behavior 1 (1-1 or 1-2), indicating less molecules went through Behavior 2 than Behavior 1. The ~0.80 E to ~0.70 transitions (circle 2) represent the refolding of a compact G4 to a different conformation during the first 5 minutes post KCl introduction. (See Supplementary Results for more detail).

Gray et al[39] utilized time dependent CD to identify G4 folding intermediates that snap into a G-hairpin within 1 minute of K^+ exposure, but then take hours to fold into a stable hybrid G4. Therefore, the observed rise in dynamic trajectories with smFRET cation exchange may be due to the formation of a G-hairpin-like short-lived intermediate species and refolding into other G4 conformations. However, the mechanism of G4 cation exchange itself remains unknown. It is possible that the G4 remains folded and

the cations flow through the central channel. It could also be that the G4 unfolds, releases the cations, allows new cations to bind, and then the G4 refolds. Behavior 1 in our data suggests that some G4s have the cation replacement occur through near complete G4 unfolding. The drop to 0.45 E shows that unfolding, even partially, might be necessary to allow the replacement of the cation in the central channel. If K^+ were able to move freely through the channel to replace Na^+, then given the position of the two dyes, there should be no apparent decline in the FRET efficiency like Behavior 2, as the distance between the 5' and 3' ends remains the same or decreases. Our data thus demonstrates that cation replacement in G4 may happen through at least two different paths and mechanisms. The propensity of certain G4s to "snap" fold as opposed to slower refolding and the propensity of certain G4s to unfold before refolding are not well understood at this time and may present a future challenge in understanding cation induced refolding of G4.

Slow G4 Refolding After the Initial Rapid Refolding.

Tracking the smFRET transitions at later time points post KCl introduction provides strong evidence supporting G4 slow refolding caused by cation exchange. There is a significant difference between the TDP generated from the first three transitions (Figure 2D) and the TDP generated from the first ten transitions (Figure 2E, top left panel) during and after KCl buffer exchange. The TDP from the first ten transitions is almost symmetric across the diagonal line, indicating all the other transitions after the first three transitions occurred between G4 conformations with different compactness, and without undergoing an unfolding event (0.45 E) very often. This result implies that the slow refolding process after the initial 3 events occurred in a random sampling fashion, without a significant preference of path but eventually reached the same conformation. Comparing the dwell time plots generated from the 5 minutes long KCl buffer exchange movie with the dwell time plots from later time points (Figure 2E) further supports that, as a G4 is allowed to incubate in KCl, the number of dynamic molecules and transitions decreases with time, as the number of static trajectories at 0.75 E increases (see Supplementary Results for more detail). Overall, the combination of dwell time plots and TDPs show the shift from rapidly occurring dynamic events to longer lived static events over the first hour of K^+ replacing Na^+. By 60 minutes, almost no transitions occurred during the 2 minutes recording time. It can thus be surmised that the 41% of molecules that did not *initially* refold in the presence of K^+ still refolded later.

Cation Exchange Refolding and Slow Cooling Produce Different Conformation Distributions.

One unexpected observation is that the dwell time plot and TDP at 60 minutes after KCl buffer exchange in 4R-TTAG is different to the dwell time plot from KCl annealed 4R-TTAG. The dwell time plot from data collected at 60 minutes post cation exchange does not have the multiple FRET populations observed in KCl annealed sample. The TDP at 60 minutes post cation exchange has remarkably lower density than the annealed sample while the states involved in the transitions are the same. These

differences suggest that, for at least some molecules, the conformations formed in the heat annealing process and the conformations formed in the refolding process are not the same. Recent work by T. Paul et al[63] shows that vectorially folded G4s and nascently folded G4s prefer different conformations. Consistent with their report, our data suggests that cation exchange changes the G4 folding path, limiting the final state a molecule may reach, thus all fluctuating populations were reduced.

Direct K^+ Introduction Has Faster Folding Rate and Different Path than Cation Exchange.

To further interrogate the differences in annealed versus refolded G4s, we used smFRET to study folding from random coil to G4 at 25°C, which mimics the folding of nascent telomeric ssDNA and may reveal different folding pathways molecules take. We annealed 4R-TTAG in 10 mM Tris and monitored smFRET signal change responding to KCl or NaCl buffer introduction. The initial smFRET data collection of Tris annealed 4R-TTAG was conducted with imaging buffer containing Li^+ instead of Na^+, as described in Material and Methods, to ensure no Na^+ was present to induce undesired G4 folding. As expected, Tris annealed 4R-TTAG exhibited a single population centered at 0.37 ± 0.03 E, indicating random coil state. The smFRET histogram at 5 minutes post 100 mM KCl introduction shows a single peak centered at 0.71 ± 0.02 E, indicating that all G4s have responded and folded. By two hours, this high FRET efficiency population had not changed (Figure 3A&B, right column). Introducing Na^+ instead of K^+ to Tris annealed sample shows a similar pattern of smFRET histogram change, as the main peak center changed from 0.37 ± 0.03 E to 0.62 ± 0.02 E at five minutes (Figure S7). Selected salt introduction smFRET trajectories can be seen in Figure S12. These results show that cation introduction is faster than cation exchange and may induce a different folding path.

To illustrate the different initial folding paths after K^+ introduction, we generated time-dependent heat maps from the smFRET signal during and after the initial K^+ introduction. In the time-dependent heat maps (Figure 3C), the FRET efficiency values of all the single-molecule trajectories were combined to give the occurrence of each FRET efficiency value at each second. Detailed interpretation of the heat maps can be found in Supplementary Results. In general, introducing KCl to the Tris annealed G4-TTAG caused a sharp “jump” of FRET efficiency within 2 seconds, as opposed to the slow initial transition that took about 15 seconds in K^+ exchange. Direct introduction of KCl to Tris annealed 4R-TTAG also created a broad distribution of FRET signal that persisted, as opposed to the narrower distribution of Na^+ to K^+ exchange which further narrowed post 150 seconds. This result strongly suggests that the existing structure in the presence of salt can influence the folding pathway and refolding rate. An explanation for this effect may lie in kinetic “traps,” where the random coil DNA collapses into a variety of conformations upon encountering the cation at room temperature, leading to the observed wide distribution of FRET efficiencies. Some of these conformations are less prone to refolding compared to the conformations induced by K^+ exchange because they fall into kinetic traps on the folding path. The dynamically refolding

G4s in Na^+ annealed samples provide a better starting point than random coil and prevent the low energy misfolding "traps" on the folding path to a stable K^+ G4.

Competitive Binder C2 Indicates Presence of Accessible Population.

The telomeric overhang binding protein POT1 and telomerase bind to telomeric overhang G-rich DNA in a single stranded form, thus accessibility of the telomeric overhang is important for telomeric protein association. The slow refolding phenomena and the kinetic trap described in the previous sections lead to the question of how telomeric DNA accessibility changes during folding and refolding. Therefore, we tested the accessibility of the telomeric DNA at different folded or refolded states with a complementary strand C2, $(CCCTAA)_2$.C2 binds with two repeats of telomeric G-rich sequence, forming a 12 bp duplex with a T_m of approximately 43°C, as calculated through the C_t dependency of T_m using 1-7 μM of C_t in our binding experiments[43]. C2 was chosen because it provides the most sensitive detection to the competition between salt refolding and duplex formation (see Supplementary Results for more detail). Given the similar melting points for this duplex and the Na^+ annealed G4, it could be assumed that neither G4 nor duplex formation is enthalpically favored, so there could be competition at sufficiently high concentrations of C2. On the other hand, the K^+ annealed G4 melts at significantly higher temperatures, at around 60 °C. Thus, we expected C2 would be unable to unfold the K^+ annealed G4s as previous work by our lab shows that C2 does not readily unfold stably folded K^+ G4s [46].

We introduced 1 μM C2, consistent with our earlier work, at different times during the salt replacement process to test at what time the G4s become sufficiently well folded enough to resist C2. All the smFRET histograms were collected 5 minutes post C2 addition, as there was not much change in the histograms after prolonged incubation with C2. As shown by the smFRET histograms in Figure 4A and S8A, adding C2 4R-TTAG at different time points of Na^+ to K^+ exchange generated a new population with very low FRET efficiency (centered at 0.20 ± 0.02 E). This low FRET efficiency population is consistent with the reported double helix structure that has a longer end-to-end distance than a random coil state[64, 65]. Therefore, the ratio of this new population can be used to quantify the DNA that is accessible to C2, which changed depending on the initial folded state of 4R-TTAG and cation incubation time (see Figure S8A). Adding C2 with KCl buffer to NaCl annealed 4R-TTAG induced 80 ± 10 % of the population to be at the 0.20 E unfolded state and left about 20% of the molecules unchanged (Fig 4A top panel). The ~20% population remaining resistant to unfolding at co-introduction of C2 and 100 mM KCl might lead to an interpretation that the Na^+ annealed G4s are exhibiting Behavior 3 (no immediate response to K^+), thus remaining folded stably enough to resist C2 unfolding. This interpretation is proved unlikely as C2 can unfold all the G4 in NaCl (Figure S8A top right). A more likely explanation is that the cation exchange in some molecules happens faster than the C2 binding, and C2 cannot unfold these "snap" folded G4 in KCl. This C2-resistant population increased as the 4R-TTAG was incubated in KCl

longer, which reached ~80 % at 120 min post KCl introduction. The persistence of the 20% unfolded population at 120 minutes suggests that there is always a population of refolded G4s susceptible to unfolding by C2. Comparing this to the earlier report stating that KCl annealed G4 are not susceptible to unfolding by C2[46], our data indicates that some refolded G4 conformations have a different accessibility to KCl annealed G4. Work by Paul et al showed that vectorial folding induced by helicases on telomeric ssDNA leads to less stably folded G4s than G4s that fold nascently in the presence of 100mM KCl [63]. They also suggest that the difference in conformation promotes higher accessibility of the ssDNA to telomeric proteins. Consistent with their report, our results suggests that K^+-induced refolding of telomeric G4s requires transient unfolding of G4, thus the cation exchange equilibrium between Na^+ and K^+ may also play a role in telomere accessibility to proteins and telomerase at different time point, perhaps a biological "clock" in G4 folding guarding the accessibility of the telomeric overhang.

To determine if the snap folding of random coil in KCl (see Figure 3) creates a different accessibility than refolding, C2 binding experiments were also performed with Tris annealed 4R-TTAG during KCl buffer incubation. The co-introduction of K^+ and C2 to Tris annealed 4R-TTAG generated 60 ± 3 % of molecules to be in the 0.2 E duplex form and ~40% of molecules in a 0.68 E folded G4 state (Figure 4A, top right). This result means that some of the initial "snap folded" conformations formed in K^+ are stable enough to resist C2, even though they may not be the most stable conformation and may undergo refolding later. This is consistent with the previous section showing that folding in K^+ introduction is faster than refolding in K^+ exchange. C2 unfolded population also decreased with increased time of KCl incubation in Tris annealed 4R-TTAG, similar to the K^+ exchange C2 binding result. Therefore, it can be surmised that slow refolding still occurs in the K^+ introduction cases. Interestingly, although Figure 4B shows a drastic reduction in the C2 unfolded population between 5 and 120 minutes for Tris annealed 4R-TTAG incubation in KCl, the K^+ introduction G4 folding histograms between 5 and 120 minutes (Figure 3A&B, right column) do not show such a drastic difference. This difference between the C2 binding and G4 folding histograms suggests that subtle conformational changes that were not obvious in the folding histograms were highlighted in the presence of C2. This trend, though faint, is also present in the case of Na^+ introduction where initial cointroduction of NaCl and C2 did not lead to any noticeable folded population, but incubation in NaCl for 120 minutes followed by C2 introduction leads to ~15% unfolding resistant population (see Supplementary Results for more detail).

Because a C2 accessible population persists even at 120 min of K^+ incubation regardless of starting from NaCl or Tris annealed 4R-TTAG, we propose that refolding may not be complete by 2 hours. This phenomenon could potentially also be explained by an inherently misfolded Na^+ population that is incapable of refolding in the presence of K^+ but is capable of being unfolded by C2. If cation exchange occurs through cation flow through the central channel and if the antiparallel conformation of the Na^+ G4

is in the basket type, with a diagonal loop spanning the central channel, this could explain why K^+ is not able to replace the Na^+ but C2 is able to unfold the G4.

Concentration Ratios of K^+ Changes Path/Pattern to Refolding

We have extensively studied the complete replacement of Na^+ by K^+. But questions remain: 1) Is complete replacement of K^+ necessary to induce the short opening to 0.4 FRET or is it an intrinsic property of a Na^+ annealed G4? 2) Is the slow refolding a unique principle of complete replacement cation exchange? and 3) Does the salt ratio encourage G4s to fold with both cations? Considering the different cellular Na^+/K^+ ratios in different cell types and during physiological responses[66-71], answers to these questions may link to G4 stability and telomere accessibility in different cell types and states. To answer these questions, we conducted smFRET buffer exchange experiments from NaCl annealed 4R-TTAG to buffers containing 25:75, 50:50, or 75:25 ratios of NaCl and KCl while keeping the total cation concentration at a constant 100 mM.

Figure 5A and S10 show the smFRET histograms collected after introducing buffers containing different Na^+/K^+ ratios. In each cation ratio, introducing the new buffer caused the migration to a higher FRET state as in the complete K^+ exchange experiment. However, the peaks in the histograms had different centers and distributions during the first 30 minutes (see Supplementary Results for more detail). smFRET trajectories showed that the quick unfolding event (to 0.45 E) occurred across all cation ratios tested. The number of molecules that underwent refolding was the same as the complete K^+ exchange. Figure 5B summarizes the center of the main peaks from smFRET histograms at different time points. Unexpectedly, among all the cation ratios tested, the 25:75 Na^+/K^+ ratio has the shallowest slope of the peak center change, while being the most different to the complete K^+ replacement.

It is interesting to note that none of the cation ratios tested seemed to induce a shoulder in smFRET histograms at 5-15 minutes as the complete cation exchange did, although smFRET trajectories showed many molecules did go through the 0.82 E state but refolded to the 0.71 E state faster than the complete K^+ exchange. This may mean that the sudden influx of high K^+ above a particular Na^+/K^+ ratio is responsible for inducing the “snap” folded high FRET population that takes longer to refold. The different G4 folding path obtained from different cation ratios may be caused by the formation of hybrid G4 containing both Na^+ and K^+ as intermediates before reaching the final stable state. Further studying this effect requires a more sensitive method and is beyond the scope of this report. Overall, our results revealed that the conformation rearrangement of telomeric G4 is highly dependent on the ratio of Na^+ and K^+ the DNA encounters. The histogram changes between 30 and 120 minutes suggests that the principle of slow refolding is not unique to complete cation exchange but of the concept of G4 rearrangement itself.

Lastly, we also performed smFRET cation exchange on replacing the buffer of KCl annealed 4R-TTAG with a buffer containing 100 mM NaCl. Interestingly, we observed a shift of smFRET histogram from the 0.71 E to a lower FRET state. The shift also reached the 0.62 E peak similar to the NaCl annealed peak by 120 minutes with the majority of refolding complete by 30 minutes (Figure S9). This result seems to contradict the established view that K^+ is a better stabilizing cation than Na^+ and may suggest that ion binding in the central channel may be transient. Currently, we are not certain why Na^+ is capable of displacing K^+, but this presents a promising new path toward understanding cation induced refolding of G4. This leads further credence to the notion that G4 unfolding and refolding is a time-dependent process and may have biological significance in the cell cycle and replication. If the telomeric overhang is only accessible for 30 minutes, then any protein action will need to be initiated within 30 minutes.

CONCLUSION

Our data clearly shows that K^+ induced a slow G4 refolding and a gradual decrease in the G-rich strand accessibility. This slow refolding phenomenon may explain the inconsistent G4 folding and binding reports in literature. For example, if a telomeric G4 was annealed in NaCl and a binding protein was introduced with KCl, the protein would have a higher chance to bind and unfold the G4[13], whereas a telomeric G4 annealed in KCl cannot be unfolded by the same protein in KCl[59]. We have used DSC, CD, and smFRET to show that, in accordance with literature, K^+ is a better G4-stabilizing cation than Na^+. This would suggest that in constant cationic conditions, K^+ G4s have a higher tendency to remain folded in stable hybrid conformations, while Na^+ G4s have a higher tendency to refold into the same or different antiparallel conformations.

However, there have been conflicting reports on the stability of G4 in various conditions. For example, we observed that KCl annealed G4s had only 6% dynamic trajectories, which is consistent with the majority of smFRET reports on telomeric G4, while reports by Lee et al.[72] reported KCl annealed G4 having 48% of molecules with dynamic smFRET trajectories in 100 mM KCl buffer. One possible explanation of such high dynamics in smFRET is the fluorescent dye position on a flapping end. While most of the G4 smFRET research has been done with one dye at the 3' sugar or phosphate of GGG, the research reported high dynamics had one dye attached to the 3' end of a TTAG sequence beyond the last GGG. As shown by our comparison between 4R and 4R-TTAG thermodynamic profiles, the TTAG tail contributes to an unfavorable entropy on G4 stability, which suggests that the TTAG tail might be flapping around while the rest of G4 is intact. Our work in this report demonstrates the complex nature of telomeric G4 stability and dynamics, which may help to explain the conflicting reports in the field.

When the telomeric G-rich sequence encounters K^+, such as buffer exchange from 100 mM NaCl to 100 mM KCl, refolding initially happens quickly but might still be incomplete by 2 hours. The distinct behaviors in response to KCl introduction may be related to the stability of the initial Na^+ G4 conformation. A delayed response to K^+ exchange suggests that some Na^+ G4 conformations may be stable enough to resist KCl introduction initially. The differences in dynamic behavior between KCl annealed G4s and cation exchanged refolded KCl G4s suggests that G4s have inherent dynamic behaviors that decrease through refolding, settling in an energy minimum wherein the G4 no longer refolds. This model is supported by the decrease in dynamic behaviors over time and the decrease in accessibility to a shorter complementary strand. As shown in our complementary strand binding assays, the shorter complementary strand C2 unfolded nearly every G4 in NaCl regardless of NaCl incubation time, whereas incubation in KCl decreases the C2 unfolded population gradually to 20% over two hours. These results may suggest that the G4 refolding caused by cations makes the sequence vulnerable to C2 attack.

Further complicating the nature of cation-induced refolding is the finding that salt exchange can happen in the reverse direction, from KCl to NaCl. It would seem counterintuitive that a stable KCl annealed G4 would refold in the presence of a less stabilizing salt, but our data for 4R-TTAG and 4R-1R indeed show that this is the case (Figure S9). Investigating the shift to a less stable conformation may elucidate a mechanism of increasing accessibility of the telomeric end.

Binding of proteins to G4-forming DNA may depend on both sequence and structure (or conformation) of the DNA. Although it is intuitive to think the sequence of an unstructured ssDNA will contribute to the specific binding of proteins, the sequence of G4-forming DNA also affects the conformation and stability of the G4 it folds into, thus altering the sequence accessibility. Work has been done on substituting bases in telomeric and other G4s to study interactions with G4-binding proteins. In telomeric G4 annealed in 100 mM KCl, changing a single T in the TTA loop to a thymine glycol residue doubled the fraction of G4 accessible to POT1 unfolding, while changing the T to a C did not significantly alter the accessibility[59]. Similarly, inducing oxidative damage or substituting a G in a GGG run to a C made approximately 90% of G4s accessible to POT1 binding[14, 59]. Recent work by J. Lee et al[72] sought to investigate binding of the cancer related protein BRCA2 to telomeric G4 to determine whether G4 acts as a “gatekeeper” that regulates access to telomeric ssDNA. They proposed that BRCA2 binds preferentially to G-triplexes (G3). However, as triplexes are intermediates in the G4 refolding pathway, the accessibility of this intermediate depends on the surrounding environment. Since we demonstrated that the folding path of telomeric G4 changes with cation type and ratio, the lifetime of the G3 needed for protein binding is dependent on the cationic environment. The differential binding modes telomeric binding proteins exhibit, such as BRCA2 tolerating TT and TTT loops versus POT1’s preference for TTA loops, highlights the importance of DNA sequence identity in protein binding to G4-forming sequences. Further studies are needed to test if the

slow refolding phenomenon exists in other G4 forming sequences, and if it exists, does the sequence contribute to different refolding path and rate.

Even though the intracellular concentration of sodium and potassium is generally reported around 10 mM and 100 mM respectively, there exist several conditions which can change the ratio of the two cations and thus potentially trigger cation induced G4 refolding. G4 folding and refolding is more complex than generally thought and should not be simply relegated to K^+ being the most stabilizing cation. We have shown that the starting conformation a G4 is in, either folded in NaCl or random coil in Tris, plays a significant role in influencing the refolding path of G4 to a stable conformation. How Na^+ modulates the K^+ induced refolding kinetics is as important yet less understood than the kinetics of G4 in K^+ alone. K^+ can replace Na^+ in folded G4 and induces a slow refolding process that seems to proceed through various long-lived intermediates and may take longer than two hours to complete. The reason for this slow unfolding process remains to be studied and presents a new view into the complex dynamics of DNA secondary structure. Further investigation may be needed to discover biological relevance in regard to physiological salt imbalance disorders, such as hyponatremia, hyperkalemia, etc.

Authors Contribution

A.N.L. and H.-T. L established the idea, designed the experiments, and wrote the manuscript. A.N.L. performed all the experiments at least twice and analyzed all the data. A.S. and A.G performed smFRET and CD experiments, processed data, and contributed to the interpretation of data.

Supporting Information

Supplementary tables for thermodynamic parameters and oligonucleotide naming conventions, additional methods for characterization of G4 forming constructs, figures supporting main assertions and characterization of 4R-TTAG at 37°C, and additional text can be found online at:

Acknowledgement

This work is supported by National Science Foundation under Grant MCB-2338902. The authors would like to thank Kristen Buettner, Jarod S. Lowe, and Dr. Aaron Lucius and members of his research group for their constant feedback and constructive criticism.

Conflict of interest

The authors claim there is no conflict of interest that may affect this manuscript.

References

(1) Moyzis, R. K.; Buckingham, J. M.; Cram, L. S.; Dani, M.; Deaven, L. L.; Jones, M. D.; Meyne, J.; Ratliff, R. L.; Wu, J. R. A highly conserved repetitive DNA sequence, (TTAGGG)n, present at the telomeres of human chromosomes. *Proceedings of the National Academy of Sciences of the United States of America* **1988**, *85* (18), 6622-6626. DOI: 10.1073/pnas.85.18.6622 From NLM.
(2) Makarov, V. L.; Hirose, Y.; Langmore, J. P. Long G tails at both ends of human chromosomes suggest a C strand degradation mechanism for telomere shortening. *Cell* **1997**, *88* (5), 657-666. DOI: 10.1016/s0092-8674(00)81908-x From NLM.
(3) McElligott, R.; Wellinger, R. J. The terminal DNA structure of mammalian chromosomes. *The EMBO journal* **1997**, *16* (12), 3705-3714. DOI: 10.1093/emboj/16.12.3705 From NLM.
(4) Neidle, S.; Parkinson, G. N. The structure of telomeric DNA. *Curr Opin Struct Biol* **2003**, *13* (3), 275-283. DOI: 10.1016/s0959-440x(03)00072-1 From NLM.
(5) Bhattacharyya, D.; Mirihana Arachchilage, G.; Basu, S. Metal Cations in G-Quadruplex Folding and Stability. *Front Chem* **2016**, *4*, 38. DOI: 10.3389/fchem.2016.00038 From NLM.
(6) Varshney, D.; Spiegel, J.; Zyner, K.; Tannahill, D.; Balasubramanian, S. The regulation and functions of DNA and RNA G-quadruplexes. *Nature Reviews Molecular Cell Biology* **2020**, *21* (8), 459-474. DOI: 10.1038/s41580-020-0236-x.
(7) Kosiol, N.; Juranek, S.; Brossart, P.; Heine, A.; Paeschke, K. G-quadruplexes: a promising target for cancer therapy. *Molecular Cancer* **2021**, *20* (1), 40. DOI: 10.1186/s12943-021-01328-4.
(8) Balasubramanian, S.; Neidle, S. G-quadruplex nucleic acids as therapeutic targets. *Current Opinion in Chemical Biology* **2009**, *13* (3), 345-353. DOI: https://doi.org/10.1016/j.cbpa.2009.04.637.
(9) Chen, Y.; Yang, D. Sequence, stability, and structure of G-quadruplexes and their interactions with drugs. *Curr Protoc Nucleic Acid Chem* **2012**, *Chapter 17*, Unit17.15. DOI: 10.1002/0471142700.nc1705s50 From NLM.
(10) Nuthanakanti, A.; Ahmed, I.; Khatik, S. Y.; Saikrishnan, K.; Srivatsan, S. G. Probing G-quadruplex topologies and recognition concurrently in real time and 3D using a dual-app nucleoside probe. *Nucleic Acids Res* **2019**, *47* (12), 6059-6072. DOI: 10.1093/nar/gkz419 From NLM.
(11) Burge, S.; Parkinson, G. N.; Hazel, P.; Todd, A. K.; Neidle, S. Quadruplex DNA: sequence, topology and structure. *Nucleic Acids Res* **2006**, *34* (19), 5402-5415. DOI: 10.1093/nar/gkl655 From NLM.
(12) Arora, A.; Maiti, S. Differential biophysical behavior of human telomeric RNA and DNA quadruplex. *The journal of physical chemistry. B* **2009**, *113* (30), 10515-10520. DOI: 10.1021/jp810638n From NLM.
(13) Hwang, H.; Buncher, N.; Opresko, P. L.; Myong, S. POT1-TPP1 regulates telomeric overhang structural dynamics. *Structure* **2012**, *20* (11), 1872-1880. DOI: 10.1016/j.str.2012.08.018 From NLM.
(14) Lee, H.-T.; Sanford, S.; Paul, T.; Choe, J.; Bose, A.; Opresko, P. L.; Myong, S. Position-Dependent Effect of Guanine Base Damage and Mutations on Telomeric G-Quadruplex and Telomerase Extension. *Biochemistry* **2020**, *59* (28), 2627-2639. DOI: 10.1021/acs.biochem.0c00434.
(15) Qureshi, M. H.; Ray, S.; Sewell, A. L.; Basu, S.; Balci, H. Replication protein A unfolds G-quadruplex structures with varying degrees of efficiency. *J Phys Chem B* **2012**, *116* (19), 5588-5594. DOI: 10.1021/jp300546u From NLM.
(16) van Steensel, B.; Smogorzewska, A.; de Lange, T. TRF2 protects human telomeres from end-to-end fusions. *Cell* **1998**, *92* (3), 401-413. DOI: 10.1016/s0092-8674(00)80932-0 From NLM.
(17) van Steensel, B.; de Lange, T. Control of telomere length by the human telomeric protein TRF1. *Nature* **1997**, *385* (6618), 740-743. DOI: 10.1038/385740a0 From NLM.

(18) de Lange, T. Shelterin: the protein complex that shapes and safeguards human telomeres. *Genes & development* **2005**, *19* (18), 2100-2110. DOI: 10.1101/gad.1346005 From NLM.
(19) Palm, W.; de Lange, T. How shelterin protects mammalian telomeres. *Annual review of genetics* **2008**, *42*, 301-334. DOI: 10.1146/annurev.genet.41.110306.130350 From NLM.
(20) Ray, S.; Bandaria, J. N.; Qureshi, M. H.; Yildiz, A.; Balci, H. G-quadruplex formation in telomeres enhances POT1/TPP1 protection against RPA binding. *Proc Natl Acad Sci U S A* **2014**, *111* (8), 2990-2995. DOI: 10.1073/pnas.1321436111 From NLM.
(21) Latrick, C. M.; Cech, T. R. POT1-TPP1 enhances telomerase processivity by slowing primer dissociation and aiding translocation. *The EMBO journal* **2010**, *29* (5), 924-933. DOI: 10.1038/emboj.2009.409 From NLM.
(22) Choi, K. H.; Farrell, A. S.; Lakamp, A. S.; Ouellette, M. M. Characterization of the DNA binding specificity of Shelterin complexes. *Nucleic acids research* **2011**, *39* (21), 9206-9223. DOI: 10.1093/nar/gkr665 From NLM.
(23) Lei, M.; Podell, E. R.; Cech, T. R. Structure of human POT1 bound to telomeric single-stranded DNA provides a model for chromosome end-protection. *Nature structural & molecular biology* **2004**, *11* (12), 1223-1229. DOI: 10.1038/nsmb867.
(24) Abreu, E.; Aritonovska, E.; Reichenbach, P.; Cristofari, G.; Culp, B.; Terns, R. M.; Lingner, J.; Terns, M. P. TIN2-tethered TPP1 recruits human telomerase to telomeres in vivo. *Molecular and cellular biology* **2010**, *30* (12), 2971-2982. DOI: 10.1128/mcb.00240-10 From NLM.
(25) Theruvathu, J. A.; Darwanto, A.; Hsu, C. W.; Sowers, L. C. The effect of Pot1 binding on the repair of thymine analogs in a telomeric DNA sequence. *Nucleic acids research* **2014**, *42* (14), 9063-9073. DOI: 10.1093/nar/gku602.
(26) Hwang, H.; Opresko, P.; Myong, S. Single-molecule real-time detection of telomerase extension activity. *Scientific reports* **2014**, *4*, 6391. DOI: 10.1038/srep06391.
(27) Hwang, H.; Kreig, A.; Calvert, J.; Lormand, J.; Kwon, Y.; Daley, J. M.; Sung, P.; Opresko, P. L.; Myong, S. Telomeric overhang length determines structural dynamics and accessibility to telomerase and ALT-associated proteins. *Structure* **2014**, *22* (6), 842-853. DOI: 10.1016/j.str.2014.03.013.
(28) Bockelmann, U.; Thomen, P.; Heslot, F. Dynamics of the DNA Duplex Formation Studied by Single Molecule Force Measurements. *Biophysical Journal* **2004**, *87* (5), 3388-3396. DOI: https://doi.org/10.1529/biophysj.104.039776.
(29) Mitra, J.; Makurath, M. A.; Ngo, T. T. M.; Troitskaia, A.; Chemla, Y. R.; Ha, T. Extreme mechanical diversity of human telomeric DNA revealed by fluorescence-force spectroscopy. *Proceedings of the National Academy of Sciences* **2019**, *116* (17), 8350-8359. DOI: doi:10.1073/pnas.1815162116.
(30) Dai, J.; Carver, M.; Punchihewa, C.; Jones, R. A.; Yang, D. Structure of the Hybrid-2 type intramolecular human telomeric G-quadruplex in K+ solution: insights into structure polymorphism of the human telomeric sequence. *Nucleic Acids Res* **2007**, *35* (15), 4927-4940. DOI: 10.1093/nar/gkm522 From NLM.
(31) Liu, C.; Zhou, B.; Geng, Y.; Yan Tam, D.; Feng, R.; Miao, H.; Xu, N.; Shi, X.; You, Y.; Hong, Y.; et al. A chair-type G-quadruplex structure formed by a human telomeric variant DNA in K(+) solution. *Chem Sci* **2019**, *10* (1), 218-226. DOI: 10.1039/c8sc03813a From NLM.
(32) Parkinson, G. N.; Collie, G. W. X-Ray Crystallographic Studies of G-Quadruplex Structures. *Methods in molecular biology* **2019**, *2035*, 131-155. DOI: 10.1007/978-1-4939-9666-7_8 From NLM.
(33) Ambrus, A.; Chen, D.; Dai, J.; Bialis, T.; Jones, R. A.; Yang, D. Human telomeric sequence forms a hybrid-type intramolecular G-quadruplex structure with mixed parallel/antiparallel strands in

potassium solution. *Nucleic Acids Res* **2006**, *34* (9), 2723-2735. DOI: 10.1093/nar/gkl348 From NLM Medline.
(34) Lee, J. Y.; Okumus, B.; Kim, D. S.; Ha, T. Extreme conformational diversity in human telomeric DNA. *Proceedings of the National Academy of Sciences of the United States of America* **2005**, *102* (52), 18938-18943. DOI: 10.1073/pnas.0506144102.
(35) Carvalho, J.; Queiroz, J. A.; Cruz, C. Circular Dichroism of G-Quadruplex: a Laboratory Experiment for the Study of Topology and Ligand Binding. *Journal of Chemical Education* **2017**, *94* (10), 1547-1551. DOI: 10.1021/acs.jchemed.7b00160.
(36) Tippana, R.; Xiao, W.; Myong, S. G-quadruplex conformation and dynamics are determined by loop length and sequence. *Nucleic Acids Res* **2014**, *42* (12), 8106-8114. DOI: 10.1093/nar/gku464 From NLM Medline.
(37) Zhang, A. Y. Q.; Balasubramanian, S. The Kinetics and Folding Pathways of Intramolecular G-Quadruplex Nucleic Acids. *Journal of the American Chemical Society* **2012**, *134* (46), 19297-19308. DOI: 10.1021/ja309851t.
(38) Nguyen, T. Q. N.; Lim, K. W.; Phan, A. T. Folding Kinetics of G-Quadruplexes: Duplex Stem Loops Drive and Accelerate G-Quadruplex Folding. *The Journal of Physical Chemistry B* **2020**, *124* (25), 5122-5130. DOI: 10.1021/acs.jpcb.0c02548.
(39) Gray, R. D.; Trent, J. O.; Chaires, J. B. Folding and unfolding pathways of the human telomeric G-quadruplex. *J Mol Biol* **2014**, *426* (8), 1629-1650. DOI: 10.1016/j.jmb.2014.01.009 From NLM.
(40) Wyatt, J. R.; Davis, P. W.; Freier, S. M. Kinetics of G-quartet-mediated tetramer formation. *Biochemistry* **1996**, *35* (24), 8002-8008. DOI: 10.1021/bi960124h From NLM.
(41) Han, H.; Cliff, C. L.; Hurley, L. H. Accelerated assembly of G-quadruplex structures by a small molecule. *Biochemistry* **1999**, *38* (22), 6981-6986. DOI: 10.1021/bi9905922 From NLM.
(42) Zhao, Y.; Kan, Z.-y.; Zeng, Z.-x.; Hao, Y.-h.; Chen, H.; Tan, Z. Determining the Folding and Unfolding Rate Constants of Nucleic Acids by Biosensor. Application to Telomere G-Quadruplex. *Journal of the American Chemical Society* **2004**, *126* (41), 13255-13264. DOI: 10.1021/ja048398c.
(43) Marky, L. A.; Breslauer, K. J. Calculating thermodynamic data for transitions of any molecularity from equilibrium melting curves. *Biopolymers* **1987**, *26* (9), 1601-1620. DOI: 10.1002/bip.360260911 From NLM.
(44) Roy, R.; Hohng, S.; Ha, T. A practical guide to single-molecule FRET. *Nature methods* **2008**, *5* (6), 507-516.
(45) Hellenkamp, B.; Schmid, S.; Doroshenko, O.; Opanasyuk, O.; Kühnemuth, R.; Adariani, S. R.; Ambrose, B.; Aznauryan, M.; Barth, A.; Birkedal, V. Precision and accuracy of single-molecule FRET measurements—a multi-laboratory benchmark study. *Nature methods* **2018**, *15* (9), 669-676.
(46) Choi, B. E.; Lee, H. T. DNA-RNA hybrid G-quadruplex tends to form near the 3' end of telomere overhang. *Biophys J* **2022**, *121* (15), 2962-2980. DOI: 10.1016/j.bpj.2022.06.026 From NLM.
(47) Aznauryan, M.; Birkedal, V. Dynamics of G-Quadruplex Formation under Molecular Crowding. *J Phys Chem Lett* **2023**, *14* (46), 10354-10360. DOI: 10.1021/acs.jpclett.3c02453 From NLM Medline.
(48) Tucker, B. A.; Hudson, J. S.; Ding, L.; Lewis, E.; Sheardy, R. D.; Kharlampieva, E.; Graves, D. Stability of the Na+ Form of the Human Telomeric G-Quadruplex: Role of Adenines in Stabilizing G-Quadruplex Structure. *ACS Omega* **2018**, *3* (1), 844-855. DOI: 10.1021/acsomega.7b01649.
(49) Hardin, C. C.; Watson, T.; Corregan, M.; Bailey, C. Cation-dependent transition between the quadruplex and Watson-Crick hairpin forms of d(CGCG3GCG). *Biochemistry* **1992**, *31* (3), 833-841. DOI: 10.1021/bi00118a028 From NLM.

(50) Lim, K. W.; Ng, V. C.; Martín-Pintado, N.; Heddi, B.; Phan, A. T. Structure of the human telomere in Na+ solution: an antiparallel (2+2) G-quadruplex scaffold reveals additional diversity. *Nucleic Acids Res* **2013**, *41* (22), 10556-10562. DOI: 10.1093/nar/gkt771 From NLM.
(51) Petraccone, L.; Spink, C.; Trent, J. O.; Garbett, N. C.; Mekmaysy, C. S.; Giancola, C.; Chaires, J. B. Structure and stability of higher-order human telomeric quadruplexes. *J Am Chem Soc* **2011**, *133* (51), 20951-20961. DOI: 10.1021/ja209192a From NLM Medline.
(52) Del Villar-Guerra, R.; Trent, J. O.; Chaires, J. B. G-Quadruplex Secondary Structure Obtained from Circular Dichroism Spectroscopy. *Angew Chem Int Ed Engl* **2018**, *57* (24), 7171-7175. DOI: 10.1002/anie.201709184 From NLM Medline.
(53) Vorlickova, M.; Kejnovska, I.; Sagi, J.; Renciuk, D.; Bednarova, K.; Motlova, J.; Kypr, J. Circular dichroism and guanine quadruplexes. *Methods* **2012**, *57* (1), 64-75. DOI: 10.1016/j.ymeth.2012.03.011 From NLM Medline.
(54) Kolesnikova, S.; Curtis, E. A. Structure and Function of Multimeric G-Quadruplexes. *Molecules* **2019**, *24* (17). DOI: 10.3390/molecules24173074 From NLM Medline.
(55) Luu, K. N.; Phan, A. T.; Kuryavyi, V.; Lacroix, L.; Patel, D. J. Structure of the human telomere in K+ solution: an intramolecular (3 + 1) G-quadruplex scaffold. *J Am Chem Soc* **2006**, *128* (30), 9963-9970. DOI: 10.1021/ja062791w From NLM.
(56) Tippana, R.; Hwang, H.; Opresko, P. L.; Bohr, V. A.; Myong, S. Single-molecule imaging reveals a common mechanism shared by G-quadruplex-resolving helicases. *Proc Natl Acad Sci U S A* **2016**, *113* (30), 8448-8453. DOI: 10.1073/pnas.1603724113 From NLM.
(57) Lane, A. N.; Chaires, J. B.; Gray, R. D.; Trent, J. O. Stability and kinetics of G-quadruplex structures. *Nucleic Acids Res* **2008**, *36* (17), 5482-5515. DOI: 10.1093/nar/gkn517 From NLM.
(58) Herbert, K. M.; Greenleaf, W. J.; Block, S. M. Single-molecule studies of RNA polymerase: motoring along. *Annu Rev Biochem* **2008**, *77*, 149-176. DOI: 10.1146/annurev.biochem.77.073106.100741 From NLM.
(59) Lee, H.-T.; Bose, A.; Lee, C.-Y.; Opresko, P. L.; Myong, S. Molecular mechanisms by which oxidative DNA damage promotes telomerase activity. *Nucleic Acids Research* **2017**, *45* (20), 11752-11765. DOI: 10.1093/nar/gkx789 (acccessed 1/29/2024).
(60) Hud, N. V.; Smith, F. W.; Anet, F. A. L.; Feigon, J. The Selectivity for K+ versus Na+ in DNA Quadruplexes Is Dominated by Relative Free Energies of Hydration: A Thermodynamic Analysis by 1H NMR. *Biochemistry* **1996**, *35* (48), 15383-15390. DOI: 10.1021/bi9620565.
(61) Ma, G.; Yu, Z.; Zhou, W.; Li, Y.; Fan, L.; Li, X. Investigation of Na+ and K+ Competitively Binding with a G-Quadruplex and Discovery of a Stable K+–Na+-Quadruplex. *The Journal of Physical Chemistry B* **2019**, *123* (26), 5405-5411. DOI: 10.1021/acs.jpcb.9b02823.
(62) Zhang, D.; Han, J.; Li, Y.; Fan, L.; Li, X. Aptamer-Based K(+) Sensor: Process of Aptamer Transforming into G-Quadruplex. *J Phys Chem B* **2016**, *120* (27), 6606-6611. DOI: 10.1021/acs.jpcb.6b05002 From NLM.
(63) Paul, T.; Opresko, P. L.; Ha, T.; Myong, S. Vectorial folding of telomere overhang promotes higher accessibility. *Nucleic Acids Research* **2022**, *50* (11), 6271-6283. DOI: 10.1093/nar/gkac401 (acccessed 3/1/2023).
(64) Murphy, M. C.; Rasnik, I.; Cheng, W.; Lohman, T. M.; Ha, T. Probing single-stranded DNA conformational flexibility using fluorescence spectroscopy. *Biophys J* **2004**, *86* (4), 2530-2537. DOI: 10.1016/s0006-3495(04)74308-8 From NLM.
(65) Ha, T. Single-molecule fluorescence methods for the study of nucleic acids. *Current Opinion in Structural Biology* **2001**, *11* (3), 287-292. DOI: https://doi.org/10.1016/S0959-440X(00)00204-9.

(66) Zylbertal, A.; Kahan, A.; Ben-Shaul, Y.; Yarom, Y.; Wagner, S. Prolonged Intracellular Na+ Dynamics Govern Electrical Activity in Accessory Olfactory Bulb Mitral Cells. *PLoS Biol* **2015**, *13* (12), e1002319. DOI: 10.1371/journal.pbio.1002319 From NLM.
(67) Zylbertal, A.; Yarom, Y.; Wagner, S. The Slow Dynamics of Intracellular Sodium Concentration Increase the Time Window of Neuronal Integration: A Simulation Study. *Front Comput Neurosci* **2017**, *11*, 85. DOI: 10.3389/fncom.2017.00085 From NLM.
(68) Calderon, D. P.; Fremont, R.; Kraenzlin, F.; Khodakhah, K. The neural substrates of rapid-onset Dystonia-Parkinsonism. *Nat Neurosci* **2011**, *14* (3), 357-365. DOI: 10.1038/nn.2753 From NLM.
(69) Campbell, G.; Mahad, D. Neurodegeneration in Progressive Multiple Sclerosis. *Cold Spring Harb Perspect Med* **2018**, *8* (10). DOI: 10.1101/cshperspect.a028985 From NLM.
(70) Forrest, M. D.; Wall, M. J.; Press, D. A.; Feng, J. The sodium-potassium pump controls the intrinsic firing of the cerebellar Purkinje neuron. *PLoS One* **2012**, *7* (12), e51169. DOI: 10.1371/journal.pone.0051169 From NLM.
(71) Shikata, E.; Miyamoto, T.; Yamaguchi, T.; Yamaguchi, I.; Kagusa, H.; Gotoh, D.; Shimada, K.; Tada, Y.; Yagi, K.; Kitazato, K. T.; et al. An imbalance between RAGE/MR/HMGB1 and ATP1α3 is associated with inflammatory changes in rat brain harboring cerebral aneurysms prone to rupture. *J Neuroinflammation* **2022**, *19* (1), 161. DOI: 10.1186/s12974-022-02526-7 From NLM.
(72) Lee, J.; Sung, K.; Joo, S. Y.; Jeong, J.-H.; Kim, S. K.; Lee, H. Dynamic interaction of BRCA2 with telomeric G-quadruplexes underlies telomere replication homeostasis. *Nature Communications* **2022**, *13* (1), 3396. DOI: 10.1038/s41467-022-31156-z.

Table 1.

Name	Sequence (5'-3')
4R	TGGCGACGGCAGCGAGGC(TTAGGG)$_4$/3Cy3/
4R-TTAG	TGGCGACGGCAGCGAGGC(TTAGGG)$_4$/iCy3/TTAG
4R-1R	TGGCGACGGCAGCGAGGC(TTAGGG)$_4$/iCy3/TTAGGG
G18mer-cy5	GCCT/iCy5/CGCTGCCGTCGCCA/3Bio/
C2	(CCCTAA)$_2$
G2	(TTAGGG)$_2$
4R-Sp9-1R	(TTAGGG)$_4$/Sp9/TTAGGG
4R-Sp18-1R	(TTAGGG)$_4$/Sp18/TTAGGG
No-Handle-4R	(TTAGGG)$_4$
No-Handle-4R-1R	(TTAGGG)$_4$/iCy3/TTAGGG
No-Handle-5R	(TTAGGG)$_5$
No-Handle-4R-TTAG	(TTAGGG)$_4$/iCy3/TTAG

Table 1. Sequences of DNA oligonucleotides consisting of telomeric repeats. /3Cy3/ represents the 3' Cy3 fluorophore modifications. /iCy3/ and /iCy5/ represent the internal Cy3 and Cy5 modifications. /3Bio/ represents the 3' Biotin modification. /Sp9/ and /Sp18/ represent internal polyethylene glycol linkers designed to mimic the distance and flexibility of the internal Cy3 and Cy5 fluorophores.

Table 2

Molecule	K^+				Na^+			
	Tm (°C)	**ΔH (kcal/mol)**	**ΔG (kcal/mol) @ 25 °C**	**ΔG (kcal/mol) @ 37 °C**	**Tm (°C)**	**ΔH (kcal/mol)**	**ΔG (kcal/mol) @ 25 °C**	**ΔG (kcal/mol) @ 37 °C**
No-Handle-4R	61 ± 1	-47 ± 2	-28 ± 2	-18 ± 2	50 ± 2	-40 ± 3	-20 ± 3	-10 ± 3
No-Handle-4R-TTAG	58 ± 2	-53 ± 3	-30 ± 3	-19 ± 3	43 ± 1	-39 ± 2	-16 ± 2	-5 ± 2
No-Handle-5R	56 ± 1	-52 ± 2	-29 ± 2	-18 ± 2	45 ± 1	-43 ± 2	-19 ± 2	-8 ± 2

Table 2. Thermodynamic profiles obtained from DSC. All the experiments are conducted in 10 mM Tris-HCl, pH 7.4, with 100 mM of NaCl or KCl. ΔH comes from integrated peak areas in DSC. ΔG calculated as described in Methods.

Scheme 1

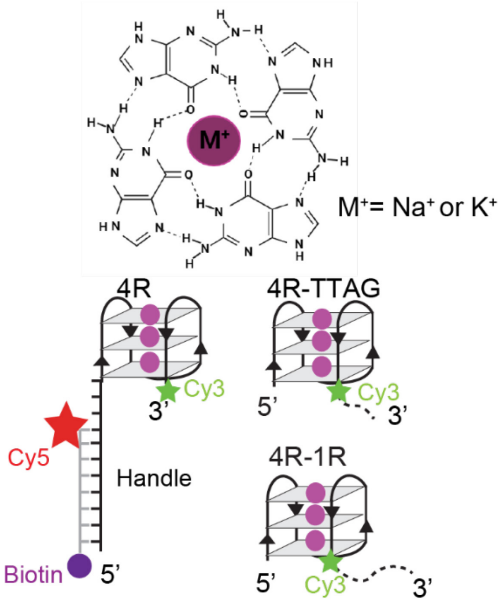

Scheme 1. Schematic representation of a G-tetrad (Top) and smFRET constructs (bottom) used in this study.

Figure 1

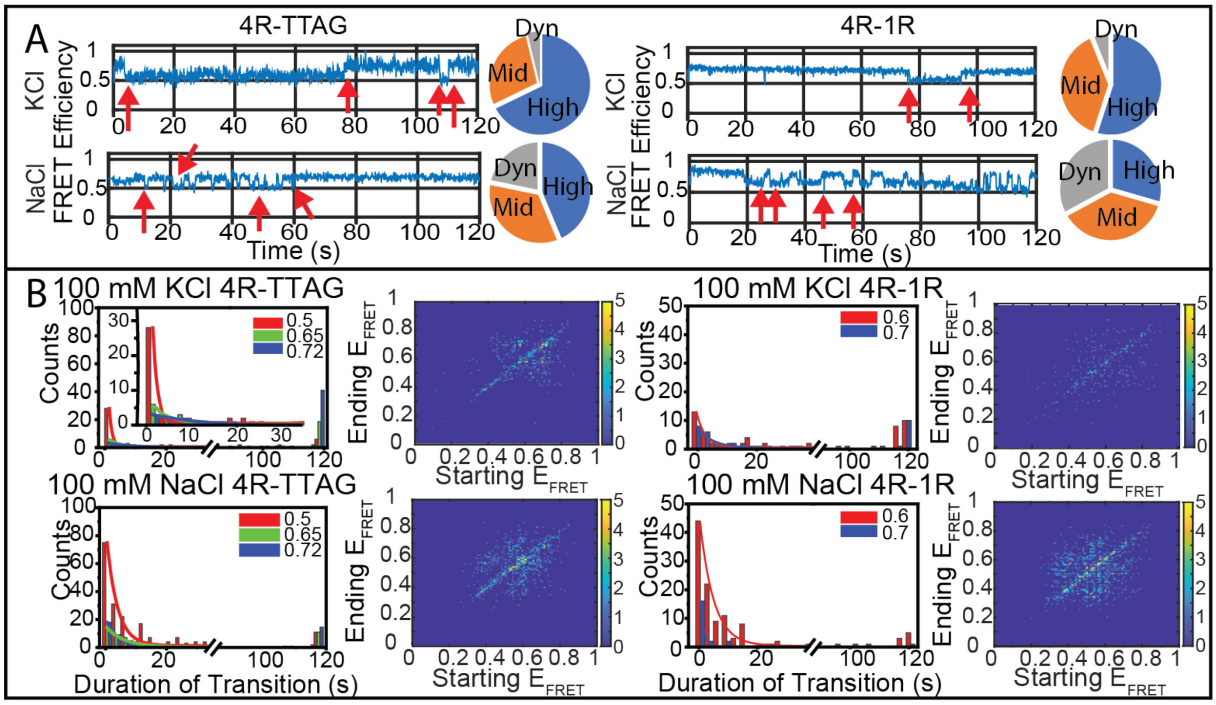

Figure 1. 4R-TTAG and 4R-1R exhibit similar types of behaviors in KCl and NaCl; 4R-1R has more dynamic events than 4R-TTAG. A. smFRET trajectories of 4R-TTAG (left) and 4R-1R (right) in 100 mM KCl (top) or NaCl (bottom). Red arrows indicate dynamic events. B. Dwell time plots and TDPs showing the number and length of transitions in either 100mM NaCl (red) and 100mM KCl (blue) for 4RTTAG (left) and 4R-1R (right). *n* = 200 molecules. All experiments conducted in 100 mM NaCl or KCl and 10 mM Tris-HCl pH 7.5. TDPs for each construct show the range of FRET efficiencies sampled in each cation. *n*= 200 molecules. Only the first ten transitions of each smFRET trajectory were plotted to avoid overwhelming the plot with molecules with high numbers of transitions within the 2 minutes recording time. The number of events is normalized to the number of molecules to generate the frequency of an event.

Figure 2

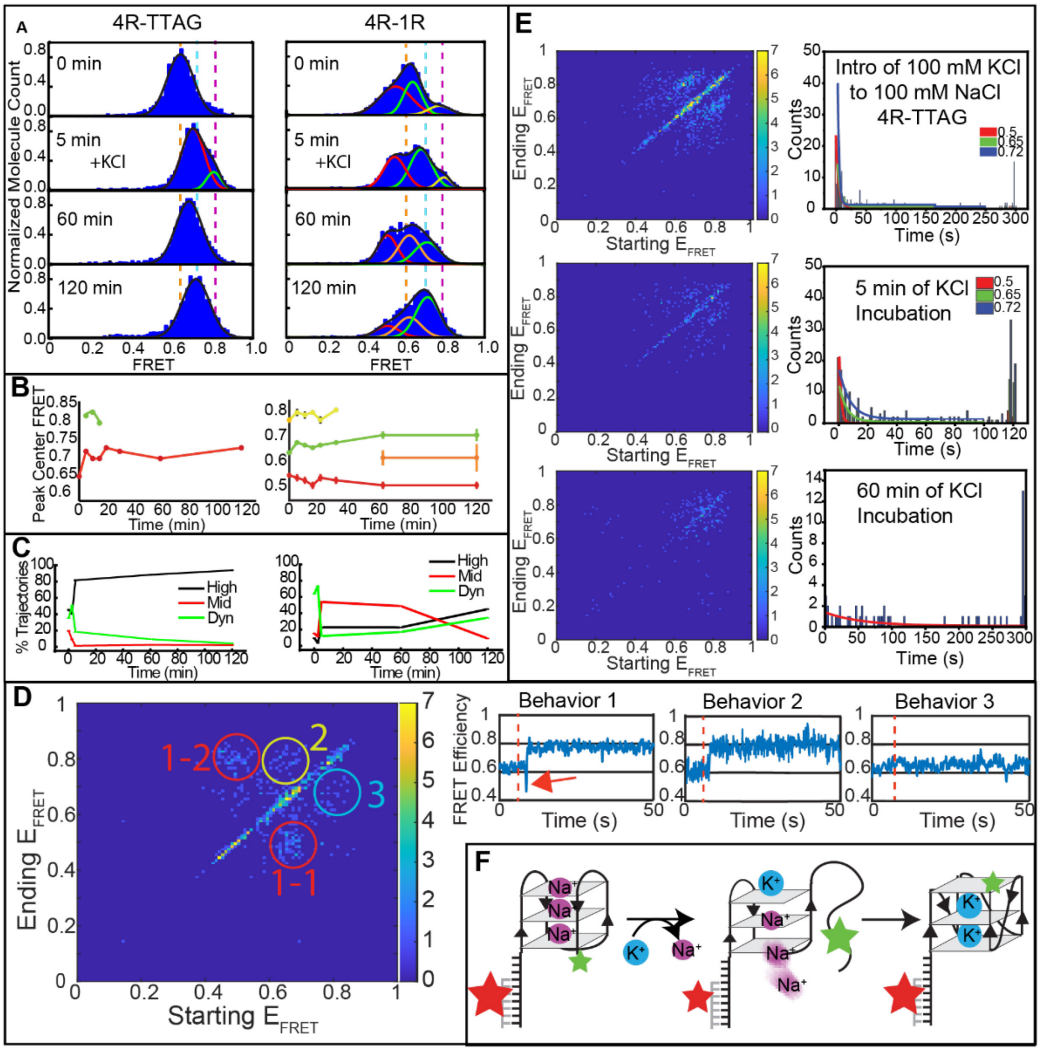

Figure 2. KCl Induced G4 Refolding Causes Shift to Higher FRET State, Formation of Different Populations, and Lowers Percentage of Dynamic FRET Trajectories. A. FRET histograms showing effects of 100mM KCl incubation with 100mM NaCl annealed 4R-TTAG (left) and 4R-1R (right) Timepoints refer to time of KCl incubation after introduction. B. FRET peak centers for 4R-TTAG (left) and 4R-1R (left) across two hours. Error bars for 4R-1R represent standard deviation across 3 repeats of cation replacement. C. % change in FRET trajectories over 2 over of KCl incubation. Colored lines indicate the change in High (black), mid (red) and dynamic (green) trajectories over 2 hours. D. Heat map generated from first 3 transitions from >200 trajectories. E. Dwell time plots (left) and TDPs (right) of 100 mM NaCl annealed 4R-TTAG refolding in 100 mM KCl at introduction, five, and sixty minutes of KCl incubation. Dwell time plots show decreasing numbers of transitions overall, with shorter (<20 sec) transitions leveling off dramatically and longer (>60 sec) transitions becoming predominant. TDPs constructed from first 10 transitions from >200 trajectories show multiple transitions occurring during introduction of KCl that then decrease over an hour. F. Proposed mechanism showing K^+ induced refolding of G4 from antiparallel to parallel.

Figure 3

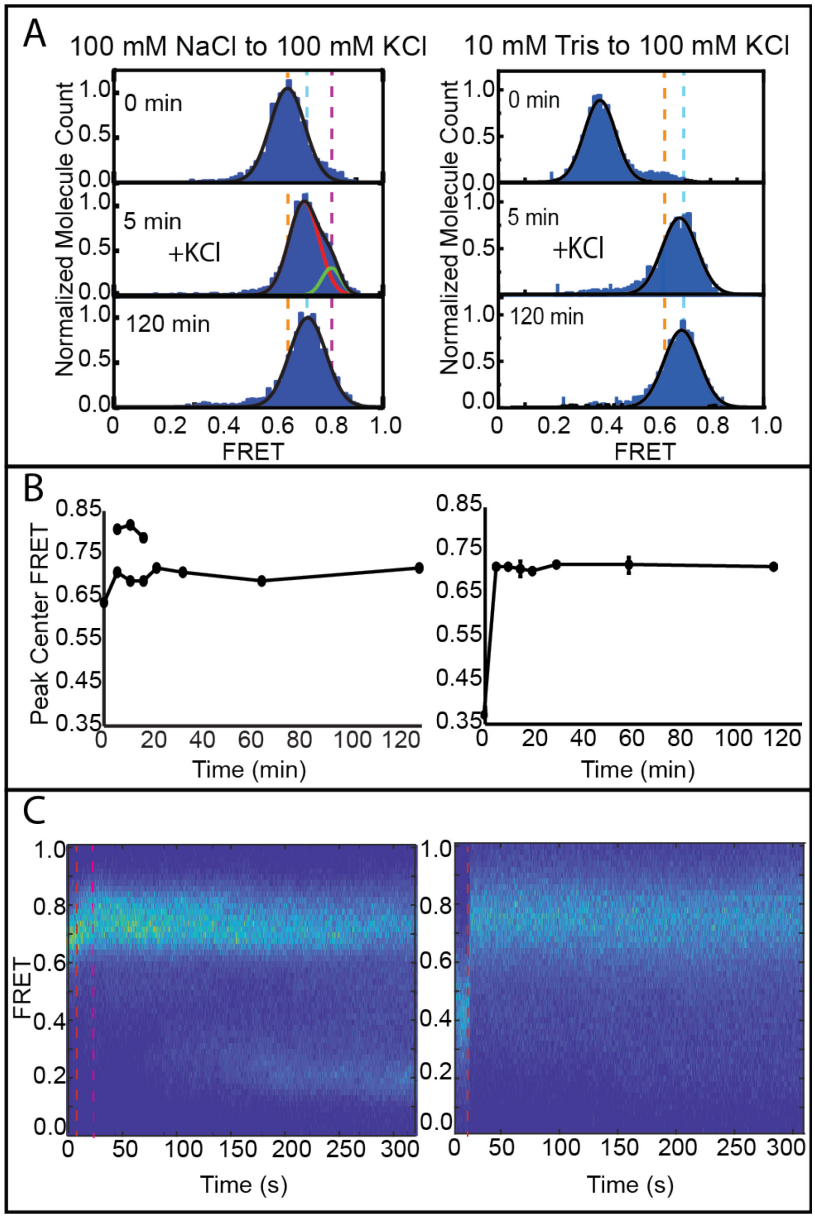

Figure 3. Direct introduction of KCl leads to snap folding of G4 into potentially unstable kinetic intermediates. A. Histograms of 4R-TTAG annealed in either 100 mM NaCl or 10 mM Tris-HCl collected at 0, 5, and 120 minutes of cation incubation in 100 mM KCl. Note that high FRET shoulder peak present in cation exchange from NaCl to KCl is not present in transition from Tris-HCl to KCl. B. Peak center FRET changes at timepoints as described in methods. C. Heat maps generated from overlaying >200 FRET efficiency trajectories collected from the five-minute-long real time flow-in movie of cation introduction. Red dashed lines indicate cation introduction, magenta line in left heat map represents end of first refolding transition.

Figure 4

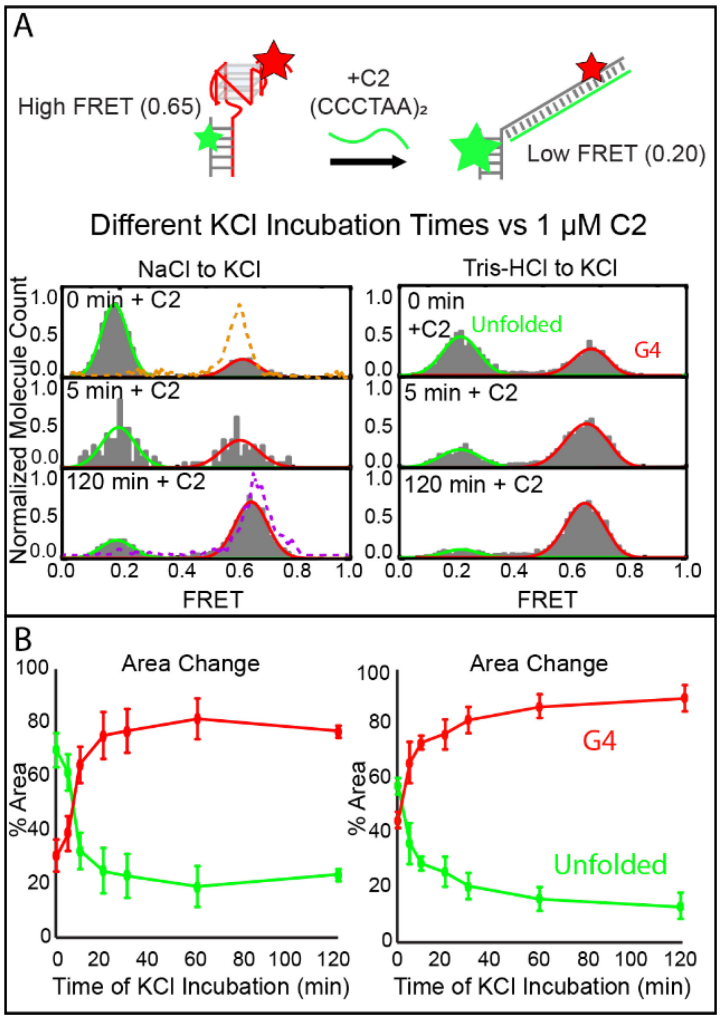

Figure 4. C2 Introduction at Different KCl Incubation Times Show that a Portion of Refolded K^+ G4s Remain Vulnerable to Unfolding A. Histograms of timepoints taken after 0, 5, and 120 min of KCl incubation followed by introduction of C2. C2 introduction induces unfolding of a small subset of the total G4 population regardless of time of KCl incubation. Top scheme depicts two major populations formed from incubation with C2, folded G4 or unfolded duplex. B. % Area change of folded vs unfolded C2 peaks over time points collected. Green line represents unfolded population, red line folded population. At 30 minutes of KCl incubation, consistent with earlier data, the amount of G4 that C2 can unfold appears to have leveled off.

Figure 5

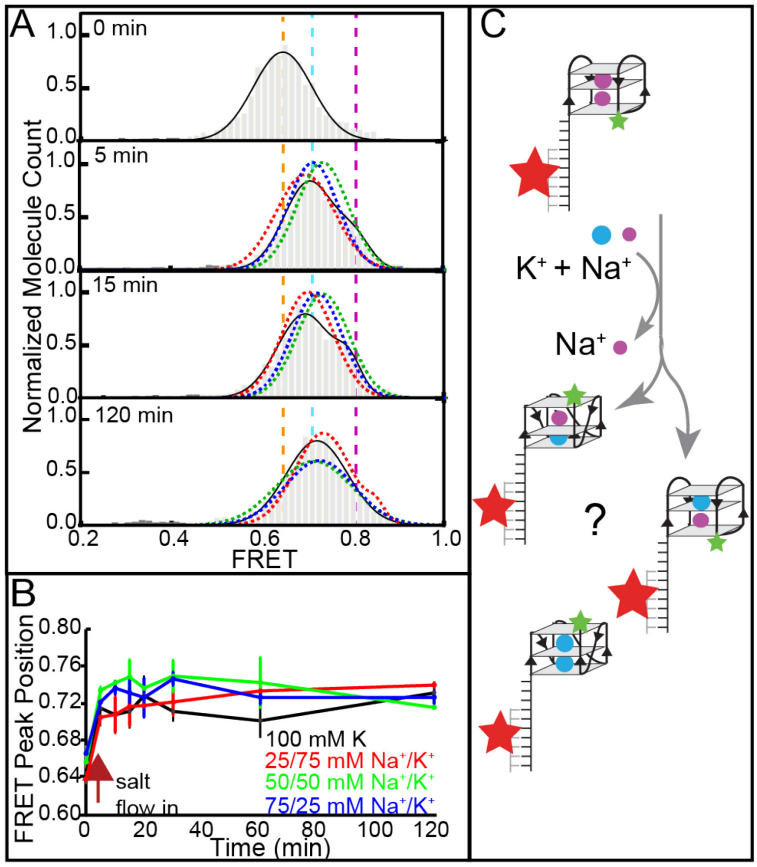

Figure 5. All Ratios Of Na/K Cause Shift To Higher FRET State, Regardless Of KCl Concentration, But The Path Is Different Between Ratios. A. Histograms for 0,5, 15, and 120 minutes of cation ratio incubation demonstrating responses to different concentrations of KCl. 25 /75 mM Na^+/K^+ (red dash), 50 /50 Na^+/K^+ (green dash), and 75/25 mM Na^+/K^+ (blue dash) overall fit lines overlaid on top of 100 mM KCl flush (grey histograms with black solid fit lines). Dashed lines represent NaCl G4 (orange), KCl parallel (cyan), and KCl antiparallel (purple) populations. B. Positions of Major FRET peaks for different salt replacement ratios, each starting from 100 mM NaCl. Each ratio was each conducted twice, with errors bars calculated from the standard deviations of the peak positions. C. Scheme showing proposed conformations resulting from incubation in various Na^+/K^+ ratios starting from initial NaCl antiparallel G4. Cointroduction of cations in differing ratios may push preference for hybrid cation G4s.

TOC Graphic